

Functional regression with multivariate responses

Ruiyan Luo

Division of Epidemiology and Biostatistics, Georgia State University School of Public Health, 140 Decatur Street, Atlanta, GA 30303
rluo@gsu.edu

Xin Qi

Department of Mathematics and Statistics, Georgia State University, 25 Park Place, Atlanta, GA 30303-3083
xqi3@gsu.edu

Abstract

We consider the functional regression model with multivariate response and functional predictors. Compared to fitting each individual response variable separately, taking advantage of the correlation between the response variables can improve the estimation and prediction accuracy. Using information in both functional predictors and multivariate response, we identify the optimal decomposition of the coefficient functions for prediction in population level. Then we propose methods to estimate this decomposition and fit the regression model for the situations of a small and a large number p of functional predictors separately. For a large p , we propose a simultaneous smooth-sparse penalty which can both make curve selection and improve estimation and prediction accuracy. We provide the asymptotic results when both the sample size and the number of functional predictors go to infinity. Our method can be applied to models with thousands of functional predictors and has been implemented in the R package `FRegSigCom`.

Key Words: functional linear regression; functional partial least squares; multivariate response; optimal decomposition; simultaneous smooth-sparse penalty; thousands of functional predictors.

Short Title: Functional regression with multivariate response

1 Introduction

Increasing interest has been shown in simultaneously predicting several quantities from a common set of predictor curves. For example, people want to predict the concentrations of several nutrition ingredients based on the near-infrared (NIR) spectrum of a corn sample. We consider the following linear regression model with multivariate response and functional predictors (MSOF),

$$\mathbf{Y} = \boldsymbol{\mu} + \sum_{j=1}^p \int_0^1 X_j(t) \mathbf{b}_j(t) dt + \boldsymbol{\varepsilon} = \boldsymbol{\mu} + \int \mathbb{B}(t)^T \mathbf{X}(t) dt + \boldsymbol{\varepsilon}, \quad (1.1)$$

where $\mathbf{Y} = (Y_1, \dots, Y_m)^T$ is an m -dimensional random vector and correlations usually exist between the Y_i 's. The functional predictors $\mathbf{X}(t) = (X_1(t), \dots, X_p(t))^T$ are random functions and without loss of generality, we assume that $X_j(t)$'s are defined in $[0, 1]$ and have mean zero. Correlation can exist between $X_j(t)$'s. The coefficient matrix $\mathbb{B}(t) = (\mathbf{b}_1(t), \dots, \mathbf{b}_p(t))^T$ is $p \times m$, where $\mathbf{b}_j(t) = (b_{j1}(t), \dots, b_{jm}(t))^T$ is m -dimensional. The integral of a vector or a matrix of functions is defined element-wise. The vectors $\boldsymbol{\mu} = (\mu_1, \dots, \mu_m)^T$ and $\boldsymbol{\varepsilon} = (\varepsilon_1, \dots, \varepsilon_m)^T$ represent the intercept and random noise, respectively. We assume that $\boldsymbol{\varepsilon}$ has mean zero and is independent of $\mathbf{X}(t)$.

Various methods have been proposed for scalar-on-function (SOF) linear regression model which is the special case of (1.1) with $m = 1$. We provide a brief review of these methods, and more thorough review can be found in Morris (2015), Wang *et al.* (2016), and Reiss *et al.* (2017). A common general approach to fit the SOF model is to expand the coefficient functions (and probably the predictor curves) using a set of basis functions, and convert the SOF model to a linear model with multiple scalar predictors. Two popular ways exist to choose basis functions. First, the forms of the basis functions do not depend on the data, such as B-spline, P-spline, and Fourier basis. This approach has been adopted by Ramsay and Dalzell (1991), Marx and Eilers (1999), Cardot *et al.* (2003b), Ramsay and Silverman (2005), Crambes *et al.* (2009), Crainiceanu and Goldsmith (2010), Goldsmith *et al.* (2011), etc. Second, basis functions are adaptively chosen from data, such as the functional principal component regression (FPCR) (Rice and Silverman, 1991; Silverman, 1996; Cardot *et al.*, 1999; Yao *et al.*, 2005b; Hall and Vial, 2006; Reiss and Ogden, 2007; Hall *et al.*, 2007; Hilgert

et al., 2013; Li *et al.*, 2013; Hosseini-Nasab, 2013), functional partial least squares (FPLS) (Preda and Saporta, 2005; Reiss and Ogden, 2007; Escabias *et al.*, 2007; Krämer *et al.*, 2008; Aguilera *et al.*, 2010; Delaigle *et al.*, 2012; Hilgert *et al.*, 2013; Li *et al.*, 2013; Hosseini-Nasab, 2013), and functional sliced inverse regression (Ferré and Yao, 2003, 2005). FPCR, using the covariance function of the predictor curves to get the basis functions, are extensively studied and have several variants (Fengler *et al.*, 2003; Kneip and Utikal, 2001; Benko *et al.*, 2009; Di *et al.*, 2009; Crainiceanu *et al.*, 2009; Greven *et al.*, 2011). FPLS, using information in both response and predictors, obtains the basis functions by maximizing the covariance between the response and functional predictors. When p is large, hybrid methods are proposed which combine basis expansion and variable selection. Zhu and Cox (2009), Lian (2013) and Kong *et al.* (2016b) perform FPCA on each functional predictor, and use PC scores as new scalar predictors to fit the model by imposing the group Lasso or group SCAD penalty. Kong *et al.* (2016a), Swihart *et al.* (2014) and Collazos *et al.* (2016) use hypothesis testing to select functional variables. Wavelet-based methods (Brown *et al.*, 2001; Zhao *et al.*, 2012, 2015; Reiss *et al.*, 2015) first transform the functional predictors to the wavelet space, and then use the wavelet coefficients as predictors to fit the model with various sparse regularization or priors imposed. In addition to the linear model, nonlinear MSOF models have been considered, such as the functional single-index model (Eilers *et al.*, 2009; Ait-Saïdi *et al.*, 2008; Ferraty *et al.*, 2011), the functional multiple-index model (James and Silverman, 2005; Chen *et al.*, 2011; Ferraty *et al.*, 2013), the functional nonparametric model (Ferraty and Vieu, 2002, 2006a; Rachdi and Vieu, 2007; Shang, 2013; Zhang *et al.*, 2014), and so on.

For the MSOF regression, only a few methods have been proposed to jointly fit all coordinates of the multivariate response. Matsui *et al.* (2008) expand both the predictor curves and coefficient functions using Gaussian basis functions, and transform the functional linear model to a linear model with multivariate response and multiple scalar predictors which is fitted using maximum likelihood estimation. Wang *et al.* (2017) assume the model $\mathbf{Y} = \mathbf{f}(X) + \boldsymbol{\varepsilon}$, where \mathbf{Y} is a multivariate response and \mathbf{f} is an unknown multivariate function of $X(t)$. FPCA is first conducted on the multivariate response to de-correlate, and each PC score is separately used as a new response and fitted using the Gaussian process regression (O'Hagan and Kingman, 1978; Rasmussen and Williams, 2006). Chaouch *et al.* (2013)

consider the nonparametric model with multivariate response and functional predictors, and propose an L_1 -median estimation method.

For multivariate response, one can separately fit a SOF regression model for each coordinate of \mathbf{Y} on $\mathbf{X}(t)$ using various methods. However, this approach ignores the correlation between the coordinates of \mathbf{Y} , which impairs the prediction accuracy and computational efficiency. One way to take account of the correlation in \mathbf{Y} is to consider the decomposition of $\mathbb{B}(t)$ of the form $\sum_{k=1}^K \boldsymbol{\gamma}_k(t) \mathbf{v}_k^T$, where $\boldsymbol{\gamma}_k(t) = (\gamma_{k1}(t), \dots, \gamma_{kp}(t))^T$ is a p -dimensional vector of functions, \mathbf{v}_k is an m -dimensional vector, and K is called the number of components. The estimates in both FPCR and FPLS belong to this type of decompositions. Aiming to estimate the regression function $\boldsymbol{\mu}_{\mathbf{Y}|\mathbf{X}} = E[\mathbf{Y}|X_1(t), \dots, X_p(t)] = \boldsymbol{\mu} + \sum_{j=1}^p \int X_j(t) \mathbf{b}_j(t)^T dt$ and make prediction, we identify the optimal decomposition of this type in population level, and characterize this decomposition using a generalized eigenvalue problem which provides an efficient way to estimate this decomposition and fit the model in practice. The stronger correlation exists between the coordinates of \mathbf{Y} , the fewer components are needed to provide good estimation of the regression function and good prediction. So our methods take advantage of the correlation structure in the response to make efficient dimension reduction. We propose different regularization for models with a small number p of functional predictors and a large p , separately. When p is large, we propose a simultaneous sparse-smooth penalty which improves the estimation and prediction accuracy by selecting a small number of predictor curves in the fitted model. We provide asymptotic results as both p and n go to infinity. Intensive simulation studies and two real data analysis show good performance of our methods, which we have implemented in the R package **FRegSigCom**.

We start with the model with $p = 1$ to introduce the optimal decomposition and our estimation method in Section 2. We extend the method to models with $p > 1$ in Section 3 and consider computational issues in Section 4. We conduct simulation studies and real data analysis in Sections 5 and 6, respectively. We provide the proofs, algorithms and additional formulas and figures in supplementary materials.

2 Regression with one functional predictor

When $p = 1$, the coefficient matrix $\mathbb{B}(t)$ in model (1.1) becomes an m -dimensional vector and is denoted as $\mathbf{b}(t)$. Then model (1.1) becomes

$$\mathbf{Y} = \boldsymbol{\mu} + \int_0^1 X(t)\mathbf{b}(t)dt + \boldsymbol{\varepsilon}. \quad (2.1)$$

2.1 Optimal decomposition for $\mathbf{b}(t)$

For model (2.1), we consider all decompositions of $\mathbf{b}(t)$ of the form $\sum_{k=1}^K \gamma_k(t)\mathbf{v}_k$, where $\gamma_k(t)$'s are functions and \mathbf{v}_k 's are m -dimensional vectors. We will identify the optimal decomposition of this form for estimating the regression function $\boldsymbol{\mu}_{\mathbf{Y}|\mathbf{X}} = \boldsymbol{\mu} + \int_0^1 X(t)\mathbf{b}(t)dt$ and predicting the response in population level. Noting that the estimates in FPCR and FPLS have this form of decomposition, afterward we will compare the optimal one with those in FPCA and FPLS.

Let $\Sigma(s, t) = \text{E}[X(s)X(t)]$ be the covariance function of $X(t)$ and define

$$\Gamma(s, t) = \int_0^1 \int_0^1 \Sigma(s, s')\mathbf{b}(s')^T\mathbf{b}(t')\Sigma(t', t)ds'dt'. \quad (2.2)$$

Let $\alpha_1(t)$ be the solution to

$$\max_{\alpha(t)} \int_0^1 \int_0^1 \alpha(s)\Gamma(s, t)\alpha(t)dsdt, \quad \text{subject to } \int_0^1 \int_0^1 \alpha(s)\Sigma(s, t)\alpha(t)dsdt = 1, \quad (2.3)$$

and $\alpha_k(t)$, $1 < k \leq K$, be the solution to

$$\begin{aligned} \max_{\alpha(t)} \int_0^1 \int_0^1 \alpha(s)\Gamma(s, t)\alpha(t)dsdt, \quad &\text{subject to } \int_0^1 \int_0^1 \alpha(s)\Sigma(s, t)\alpha(t)dsdt = 1 \\ &\text{and } \int_0^1 \int_0^1 \alpha_{k'}(s)\Sigma(s, t)\alpha(t)dsdt = 0, \quad 1 \leq k' \leq k-1. \end{aligned} \quad (2.4)$$

The (2.3) and (2.4) define a sequence of generalized eigenvalue problems with solutions $\{\alpha_k(t), 1 \leq k \leq K\}$ called the eigenfunctions. As both $\Sigma(s, t)$ and $\Gamma(s, t)$ are symmetric nonnegative definite kernel functions, the maximum values of (2.3) and (2.4) are nonnegative and denoted as $\sigma_1^2 \geq \sigma_2^2 \geq \dots \geq \sigma_K^2$. We call σ_k^2 the eigenvalue corresponding to the k -th eigenfunction $\alpha_k(t)$. Define an m -dimensional vector $\mathbf{w}_k = \int_0^1 \int_0^1 \alpha_k(s)\Sigma(s, t)\mathbf{b}(t)dsdt$ for $k \geq 1$. In the following theorem, we show that $\sum_{k=1}^K \alpha_k(t)\mathbf{w}_k$ is the optimal decomposition.

Theorem 2.1. Let K_0 denote the total number of positive eigenvalues of the generalized eigenvalue problem (2.4) and $\sigma_1^2 \geq \dots \geq \sigma_{K_0}^2 > 0 = \sigma_{K_0+1}^2 \dots$ denote the decreasingly sorted eigenvalues. The $\alpha_k(t)$'s and \mathbf{w}_k 's are defined as above.

(1). K_0 is less than or equal to m , and $(\sigma_k^2, \mathbf{w}_k)$ is also the k -th eigenvalue-eigenvector pair of the covariance matrix of $\boldsymbol{\mu}_{\mathbf{Y}|\mathbf{X}}$, for $1 \leq k \leq K_0$.

(2). The vector $\boldsymbol{\mu} + \int_0^1 X(t) \{\sum_{k=1}^K \alpha_k(t) \mathbf{w}_k\} dt$ has the smallest mean squared error in approximating the regression function $\boldsymbol{\mu}_{\mathbf{Y}|\mathbf{X}}$. Specifically, we have

$$\begin{aligned} & \mathbb{E} \left[\left\| \boldsymbol{\mu}_{\mathbf{Y}|\mathbf{X}} - \boldsymbol{\mu} - \int_0^1 X(t) \left\{ \sum_{k=1}^K \alpha_k(t) \mathbf{w}_k \right\} dt \right\|_2^2 \right] = \sum_{k=K+1}^{K_0} \sigma_k^2 \\ &= \min_{\boldsymbol{\nu}, \gamma_k(t), \mathbf{v}_k, 1 \leq k \leq K} \left\{ \mathbb{E} \left[\left\| \boldsymbol{\mu}_{\mathbf{Y}|\mathbf{X}} - \boldsymbol{\nu} - \int_0^1 X(t) \left\{ \sum_{k=1}^K \gamma_k(t) \mathbf{v}_k \right\} dt \right\|_2^2 \right] \right\}, \end{aligned} \quad (2.5)$$

where the minimum is taken over all square integrable functions $\gamma_k(t)$'s and all m -dimensional vectors $\boldsymbol{\nu}$ and \mathbf{v}_k 's.

(3). For a new observation $(X_{\text{new}}(t), \mathbf{Y}_{\text{new}})$, the predicted response vector given by $\boldsymbol{\mu} + \int_0^1 X_{\text{new}}(t) \{\sum_{k=1}^K \alpha_k(t) \mathbf{w}_k\} dt$ has the smallest prediction error as follows,

$$\begin{aligned} & \mathbb{E} \left[\left\| \mathbf{Y}_{\text{new}} - \boldsymbol{\mu} - \int_0^1 X_{\text{new}}(t) \left\{ \sum_{k=1}^K \alpha_k(t) \mathbf{w}_k \right\} dt \right\|_2^2 \right] = \sum_{k=K+1}^{K_0} \sigma_k^2 + \mathbb{E}[\|\boldsymbol{\varepsilon}_{\text{new}}\|_2^2] \\ &= \min_{\boldsymbol{\nu}, \gamma_k(t), \mathbf{v}_k, 1 \leq k \leq K} \left\{ \mathbb{E} \left[\left\| \mathbf{Y}_{\text{new}} - \boldsymbol{\nu} - \int_0^1 X_{\text{new}}(t) \left\{ \sum_{k=1}^K \gamma_k(t) \mathbf{v}_k \right\} dt \right\|_2^2 \right] \right\}, \end{aligned} \quad (2.6)$$

where $\boldsymbol{\varepsilon}_{\text{new}}$ is the noise vector in \mathbf{Y}_{new} and is independent of $X_{\text{new}}(t)$ and the original variables $(X(t), \mathbf{Y})$.

Theorem 2.1 shows that given K , the goodness of $\boldsymbol{\mu} + \int_0^1 X(t) \left\{ \sum_{k=1}^K \alpha_k(t) \mathbf{w}_k \right\} dt$ in approximating $\boldsymbol{\mu}_{\mathbf{Y}|\mathbf{X}}$ can be measured by $\sum_{k>K} \sigma_k^2$. Therefore, the faster is the decay of $\sigma_1^2 \geq \sigma_2^2 \geq \dots$, a smaller number K of components is needed to provide an adequate approximation to $\boldsymbol{\mu}_{\mathbf{Y}|\mathbf{X}}$. The decay rate of σ_k^2 's is affected by the correlation between the coordinates in $\boldsymbol{\mu}_{\mathbf{Y}|\mathbf{X}}$. Generally speaking, stronger correlation between the coordinates in $\boldsymbol{\mu}_{\mathbf{Y}|\mathbf{X}}$ leads to a faster decrease of σ_k^2 . As an example, we take $m = 20$ and consider two cases for the covariance matrix of $\boldsymbol{\mu}_{\mathbf{Y}|\mathbf{X}}$. Case 1: the (i, j) -th entry of the covariance matrix is $\rho^{|i-j|}$;

Case 2: all the diagonal elements of the covariance matrix equal to 1 and all others are ρ , where in both cases, $-1 \leq \rho \leq 1$. A larger value of $|\rho|$ indicates stronger correlation between the coordinates of $\mu_{Y|X}$. We plot the *relative approximation errors*, $\sum_{k=K+1}^m \sigma_k^2 / \sum_{k=1}^m \sigma_k^2$, versus K for the two cases, respectively, in Figure 1 which shows that a larger value of $|\rho|$ leads to a faster decay of the relative approximation error in both cases.

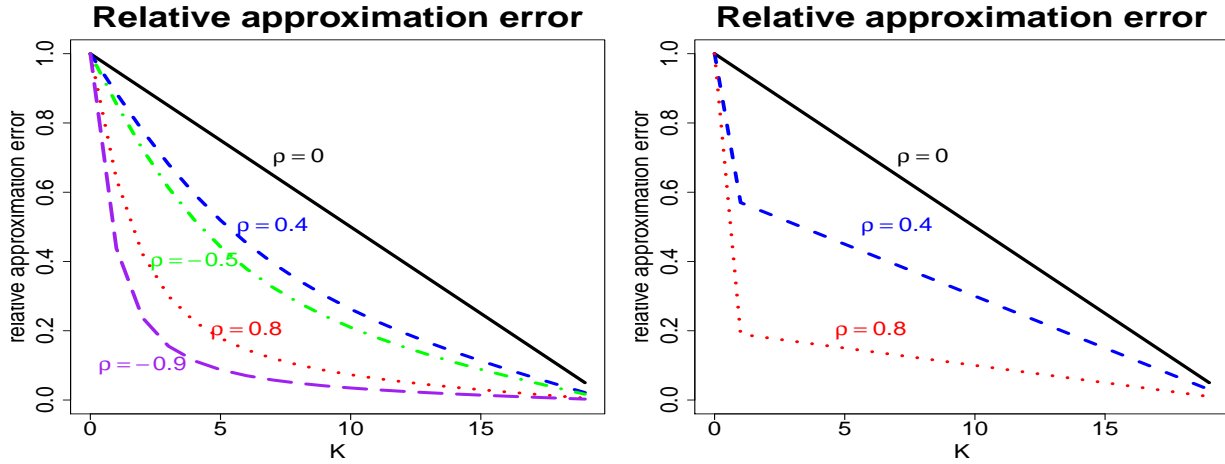


Figure 1: Two examples for the relative approximation errors of the optimal decomposition of $\mathbf{b}(t)$ versus the number K of components, where different correlation levels indicated by ρ are considered. The left plot is for the covariance matrix of $\mu_{Y|X}$ with the (i, j) -th entry equal to $\rho^{|i-j|}$; the right plot is for the covariance matrix with diagonal elements equal to 1 and off-diagonal elements equal to ρ .

Assuming that the expectation of the predictor curve is zero, the squared prediction error in (2.6) also gives the sum of variances of all the coordinates of prediction vector. The first equality in (2.6) shows that the squared prediction error consists of two parts: $\sum_{k=K+1}^{K_0} \sigma_k^2$ and $E[\|\boldsymbol{\varepsilon}_{\text{new}}\|_2^2]$. The second part is the variance of the noise vector $\boldsymbol{\varepsilon}_{\text{new}}$ which is independent of $X_{\text{new}}(t)$ and the original data $(X(t), \mathbf{Y})$. It can not be reduced when prediction is based on $X_{\text{new}}(t)$ and $(X(t), \mathbf{Y})$. The first part $\sum_{k=K+1}^{K_0} \sigma_k^2$ is due to the truncation of the decomposition $\sum_{k=1}^{K_0} \alpha_k(t) \mathbf{w}_k$ after the first K terms. It can be reduced by increasing the number K of components. However, in practice, we have to estimate $\alpha_k(t)$'s and \mathbf{w}_k 's. So in addition to the truncation error and the random error, the prediction error in practice also includes the estimation error of $\alpha_k(t)$'s and \mathbf{w}_k 's. Despite the reduction of the truncation error, a larger K leads to more functions to be estimated, which brings additional estimation error. In practice, we have to choose an appropriate K to achieve a balance between the

prediction error due to truncation and that due to estimation.

Two popular dimension reduction methods, FPCR and FPLS, also generate the decompositions of the form $\sum_{k=1}^K \gamma_k(t) \mathbf{v}_k$ for $\mathbf{b}(t)$. In FPCR, $\gamma_k(t)$'s are eigenfunctions of the covariance of the predictor curve. The FPLS extends the idea of PLS to build orthogonal components that maximize their covariance with response. There are different variants of PLS (Wold, 1973, 1975; ter Braak and de Jong, 1998; Boulesteix and Strimmer, 2006), and hence different versions of FPLS have been proposed (Goutis and Fearn, 1996; Reiss and Ogden, 2007; Krämer *et al.*, 2008; Krämer and Sugiyama, 2011; Delaigle *et al.*, 2012). For example, the FPLS implemented in software **R** is based on the work of Krämer *et al.* (2008) and Krämer and Sugiyama (2011) that finds uncorrelated latent variables to maximize the squared covariance between \mathbf{Y} and the latent variables where the length of loading vectors equal to 1. In the population level, this FPLS solves

$$\begin{aligned} \max_{\alpha(t)} \quad & \int_0^1 \int_0^1 \alpha(s) \Gamma(s, t) \alpha(t) ds dt, \\ \text{subject to} \quad & \|\alpha\|_{L^2} = 1, \quad \text{and} \quad \int_0^1 \int_0^1 \alpha_{k'}(s) \Sigma(s, t) \alpha(t) ds dt = 0, \quad 1 \leq k' \leq k-1. \end{aligned} \quad (2.7)$$

Problems (2.4) and (2.7) share a common objective function which can be expressed as

$$\int_0^1 \int_0^1 \alpha(s) \Gamma(s, t) \alpha(t) ds dt = \mathbb{E} \left[\int_0^1 X(t) \alpha_k(t) dt (\mathbf{Y} - \boldsymbol{\mu}) \right]^T \mathbb{E} \left[\int_0^1 X(t) \alpha_k(t) dt (\mathbf{Y} - \boldsymbol{\mu}) \right], \quad (2.8)$$

the sum of squared covariance between $\int_0^1 X(t) \alpha_k(t) dt$ and each response coordinate. The common restriction $0 = \int_0^1 \int_0^1 \alpha_{k'}(s) \Sigma(s, t) \alpha(t) ds dt = \text{Cov}(\int_0^1 X(t) \alpha_k(t) dt, \int_0^1 X(t) \alpha_{k'}(t) dt)$ implies that $\int_0^1 X(t) \alpha_k(t) dt$ and $\int_0^1 X(t) \alpha_{k'}(t) dt$ are uncorrelated for $k \neq k'$. But FPLS in (2.7) requires that α_k has unit length, and the region $\{\alpha(t) : \|\alpha\|_{L^2} = 1\}$ for (2.7) is the unit sphere in $L^2[0, 1]$; while (2.4) requires that $\int_0^1 X(t) \alpha_k(t) dt$ has unit variance as

$$\text{Var} \left(\int_0^1 X(t) \alpha_k(t) dt \right) = \mathbb{E} \left[\left\{ \int_0^1 X(t) \alpha_k(t) dt \right\}^2 \right] = \int_0^1 \int_0^1 \alpha(s) \Sigma(s, t) \alpha(t) ds dt = 1,$$

and the region $\{\alpha(t) : \int_0^1 \int_0^1 \alpha(s) \Sigma(s, t) \alpha(t) ds dt = 1\}$ is an ellipsoid. Hence the solutions to (2.4) and (2.7) are usually different. In Figure 2, we provide an example to illustrate the difference between the optimal decomposition and those for FPCR and FPLS. Let $X(t)$ be the Brownian motion in $[0, 1]$, and its covariance function is $\Sigma(t', t) = \min(t', t)$. Let

$\mathbf{b}(s) = (b_1(s), \dots, b_5(s))^T$ be a five-dimensional vector with $b_k(s) = \sin(k\pi t) + 2\sin((k+1)\pi t)$ for $1 \leq k \leq 5$. We draw the first three component functions used in decomposition, and the relative approximation errors to $\mu_{\mathbf{Y}|\mathbf{X}}$ versus the number K of components for each of three decomposition methods in Figure 2 which shows that our components are quite different from those in FPCR and FPLS. For each K , the optimal decomposition leads to the smallest approximation error to $\mu_{\mathbf{Y}|\mathbf{X}}$. When $K = 1$, the approximation error of the optimal decomposition is less than half of any of the other two. When $K = 5$ (the dimension of the response), the approximation error of the optimal decomposition is zero, whereas the other two still have positive errors. Indeed, Theorem 2.1 shows that the optimal decomposition can provide a perfect approximation to $\mu_{\mathbf{Y}|\mathbf{X}}$ with K not greater than the dimension of the response. This fact provides an upper bound for our choice of optimal K in practice.

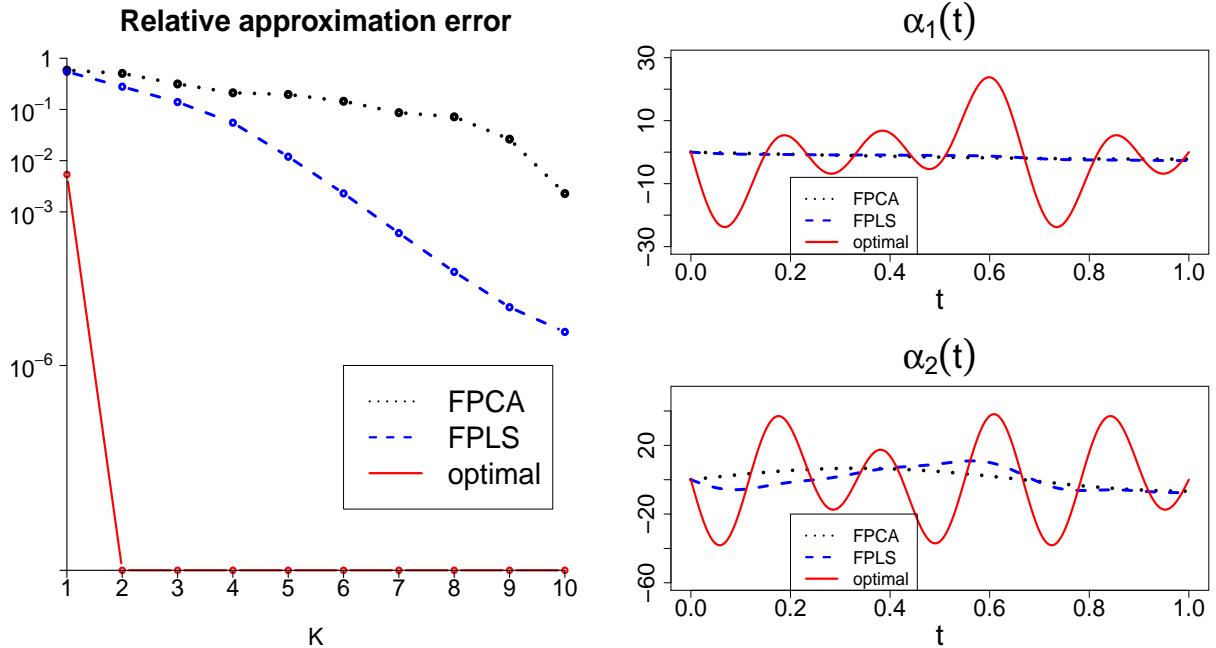


Figure 2: Comparison of the components $\alpha_k(t)$ obtained by 3 methods: FPCA, FPLS and our optimal decomposition. For comparison, all components are scaled so that $\int_0^1 \int_0^1 \alpha(s)\Sigma(s,t)\alpha(t)dsdt = 1$. *Top-left*: the first component $\alpha_1(t)$. *Top-right*: the second component. *Bottom-left*: the third component. *Bottom-right*: the relative approximation error $\mu_{\mathbf{Y}|\mathbf{X}}$ versus the number K of components for the three methods.

2.2 Estimation of the optimal decomposition

Let $\{\mathbf{Y}_\ell = (Y_{\ell 1}, \dots, Y_{\ell m})^T, X_\ell(t) : 1 \leq \ell \leq n\}$ be n independent samples from the model (2.1), and $\boldsymbol{\varepsilon}_\ell$ denote the noise in \mathbf{Y}_ℓ . Let $\bar{\mathbf{Y}}$ and $\bar{X}(t)$ denote sample means, and $\widehat{\Sigma}(s, t) = \sum_{\ell=1}^n \{X_\ell(s) - \bar{X}(s)\} \{X_\ell(t) - \bar{X}(t)\} / n$ denote the sample covariance function of predictor. Let $\widehat{\Gamma}(s, t) = [\sum_{\ell=1}^n \{X_\ell(s) - \bar{X}(s)\} \{\mathbf{Y}_\ell - \bar{\mathbf{Y}}\}^T] [\sum_{\ell'=1}^n \{\mathbf{Y}_{\ell'} - \bar{\mathbf{Y}}\} \{X_{\ell'}(t) - \bar{X}(t)\}] / n^2$. To see that $\widehat{\Gamma}(s, t)$ is an estimator of $\Gamma(s, t)$, plugging $\mathbf{Y}_\ell = \boldsymbol{\mu} + \int_0^1 X_\ell(t) \mathbf{b}(t) dt + \boldsymbol{\varepsilon}_\ell$ into the definition of $\widehat{\Gamma}(s, t)$, we have

$$\begin{aligned} \widehat{\Gamma}(s, t) &= \int_0^1 \int_0^1 \widehat{\Sigma}(s, s') \mathbf{b}(s')^T \mathbf{b}(t') \widehat{\Sigma}(t', t) ds' dt' \\ &\quad + \frac{2}{n} \sum_{\ell'=1}^n \{\boldsymbol{\varepsilon}_{\ell'} - \bar{\boldsymbol{\varepsilon}}\} \{X_{\ell'}(t) - \bar{X}(t)\} \int_0^1 \widehat{\Sigma}(s, s') \mathbf{b}(s')^T ds' \\ &\quad + \frac{1}{n^2} \left[\sum_{l=1}^n \{X_l(s) - \bar{X}(s)\} \{\boldsymbol{\varepsilon}_l - \bar{\boldsymbol{\varepsilon}}\}^T \right] \left[\sum_{\ell'=1}^n \{\boldsymbol{\varepsilon}_{\ell'} - \bar{\boldsymbol{\varepsilon}}\} \{X_{\ell'}(t) - \bar{X}(t)\} \right], \end{aligned}$$

where the last two terms converge in probability to zero as $n \rightarrow \infty$ due to the law of large numbers and the independence of $X_l(s)$'s and $\boldsymbol{\varepsilon}_l$'s. So $\widehat{\Gamma}(s, t)$ is a consistent estimator of $\Gamma(s, t)$. As the generalized eigenvalue problem (2.4) is equivalent to the following Rayleigh quotient maximization problem,

$$\begin{aligned} \max_{\alpha(t)} \frac{\int_0^1 \int_0^1 \alpha(s) \Gamma(s, t) \alpha(t) ds dt}{\int_0^1 \int_0^1 \alpha(s) \Sigma(s, t) \alpha(t) ds dt}, \quad \text{subject to } \int_0^1 \int_0^1 \alpha(s) \Sigma(s, t) \alpha(t) ds dt = 1 \\ \text{and } \int_0^1 \int_0^1 \alpha_{k'}(s) \Sigma(s, t) \alpha(t) ds dt = 0, \quad 1 \leq k' \leq k-1, \end{aligned}$$

we propose to get the estimate $\widehat{\alpha}_k(t)$ of $\alpha_k(t)$ in the optimal decomposition by solving

$$\begin{aligned} \max_{\alpha(t)} \frac{\int_0^1 \int_0^1 \alpha(s) \widehat{\Gamma}(s, t) \alpha(t) ds dt}{\int_0^1 \int_0^1 \alpha(s) \widehat{\Sigma}(s, t) \alpha(t) ds dt + P(\alpha)}, \quad \text{subject to } \int_0^1 \int_0^1 \alpha(s) \widehat{\Sigma}(s, t) \alpha(t) ds dt = 1 \\ \text{and } \int_0^1 \int_0^1 \widehat{\alpha}_{k'}(s) \widehat{\Sigma}(s, t) \alpha(t) ds dt = 0, \quad 1 \leq k' \leq k-1, \end{aligned} \tag{2.9}$$

where $P(\alpha) = \tau (\|\alpha\|_{L^2}^2 + \eta \|\alpha''\|_{L^2}^2)$, $\alpha''(t)$ represents the second derivative of $\alpha(t)$, and $\|\cdot\|_{L^2}$ denotes the L^2 norm of a function. The way we impose the penalty $P(\alpha)$ in (2.9) has been used in functional data analysis. For example, in the regularized FPCA (Section 9.3.1 of Ramsay and Silverman (2005)), a penalized objective function,

$\int \int \xi(s) \widehat{\Sigma}(s, t) \xi(t) ds dt / (\|\xi\|_{L^2}^2 + \lambda \|\xi''\|_{L^2}^2)$, is maximized over all smooth function $\xi(s)$. Imposing penalty in the denominator of the objective function, we will have a smaller value of the objective function for a rougher $\xi(s)$ with a large value of $\|\xi''\|_{L^2}^2$. So the maximizer of this objective function is a smooth function, and the larger is λ , the smoother is the maximizer. In our penalty $P(\alpha)$, the term $\|\alpha''\|_{L^2}^2$ is the smoothness penalty and plays the same role as that in the regularized FPCA. On the other hand, as $\widehat{\Sigma}(s, t)$ is estimated from a finite number of samples, it has only a finite number of positive eigenvalues. If we only impose the smoothness penalty in (2.9), the solution to (2.9) may not be unique and the solution $\widehat{\alpha}_k(s)$ can have a much larger norm than $\alpha_k(t)$, just like the overfitting problems due to multicollinearity in classic linear model. Motivated by the ridge penalty which is used to shrink the estimated coefficients and alleviate the effect of multicollinearity, we add the term $\tau \|\alpha\|_{L^2}^2$ in our penalty to control the norm of α . The parameter η tunes the relative importance between $\|\alpha\|_{L^2}^2$ and $\|\alpha''\|_{L^2}^2$ in the penalty.

Suppose that we have obtained the estimates $\widehat{\alpha}_k(t)$, $1 \leq k \leq K$. To estimate the intercept vector $\boldsymbol{\mu}$ and the vectors \mathbf{w}_k 's in the optimal decomposition, we define $\widehat{T}_{\ell,k} = \int_0^1 \{X_\ell(t) - \bar{X}(t)\} \widehat{\alpha}_k(t) dt$ for $1 \leq \ell \leq n$ and $1 \leq k \leq K$, and let $\widehat{\mathbf{T}}_k = (\widehat{T}_{1,k}, \dots, \widehat{T}_{n,k})^T$. Then we get the estimates $\{\widehat{\boldsymbol{\mu}}, \widehat{\mathbf{w}}_1, \dots, \widehat{\mathbf{w}}_K\}$ by regressing \mathbf{Y}_ℓ 's on the new scalar predictors $\widehat{\mathbf{T}}_k$'s using the following least squares problem,

$$\min_{\boldsymbol{\nu}, \mathbf{v}_k, 1 \leq k \leq K} \left\{ \sum_{\ell=1}^n \left\| \mathbf{Y}_\ell - \boldsymbol{\nu} - \sum_{k=1}^K \widehat{T}_{\ell,k} \mathbf{v}_k \right\|_2^2 \right\}, \quad (2.10)$$

where the minimum is taken over all m -dimensional vectors $\boldsymbol{\nu}$ and \mathbf{v}_k 's. As the $\widehat{\mathbf{T}}_k$'s are orthogonal, the solution to (2.10) can be explicitly given by $\widehat{\boldsymbol{\mu}} = \bar{\mathbf{Y}}$ and $\widehat{\mathbf{w}}_k = \sum_{\ell=1}^n \widehat{T}_{\ell,k} \mathbf{Y}_\ell / n$ for $1 \leq k \leq K$. Finally, we estimate $\boldsymbol{\mu}_{\mathbf{Y}|\mathbf{X}}$ by $\widehat{\boldsymbol{\mu}}_{\mathbf{Y}|\mathbf{X}} = \widehat{\boldsymbol{\mu}} + \int_0^1 X(t) \{\sum_{k=1}^K \widehat{\alpha}_k(t) \widehat{\mathbf{w}}_k\} dt$. Given a new observation $X_{\text{new}}(t)$ of the functional predictor, we predict the response vector as $\mathbf{Y}_{\text{pred}} = \widehat{\boldsymbol{\mu}} + \int_0^1 X_{\text{new}}(t) \{\sum_{k=1}^K \widehat{\alpha}_k(t) \widehat{\mathbf{w}}_k\} dt$.

3 Regression with multiple functional predictors

For model (1.1) with multiple functional predictors ($p > 1$), we first provide the optimal decomposition for the $p \times m$ matrix $\mathbb{B}(t)$ of coefficient functions in the population level.

Then we estimate this decomposition separately for two cases: a small p and a large p .

3.1 Optimal decomposition for $\mathbb{B}(t)$

Extending the decomposition in Section 2.1, for model (1.1) with $p > 1$, we consider the decomposition of $\mathbb{B}(t)$ of the form $\sum_{k=1}^K \boldsymbol{\gamma}_k(t) \mathbf{v}_k^T$, where $\boldsymbol{\gamma}_k(t) = (\gamma_{k1}(t), \dots, \gamma_{kp}(t))^T$ is a p -dimensional vector of functions, and \mathbf{v}_k is an m -dimensional vector. To find the optimal one of such form, we define two $p \times p$ matrices of kernel functions

$$\boldsymbol{\Sigma}(s, t) = \mathbb{E}[\mathbf{X}(s)\mathbf{X}(t)^T], \quad \boldsymbol{\Gamma}(s, t) = \int_0^1 \int_0^1 \boldsymbol{\Sigma}(s, s') \mathbb{B}(s') \mathbb{B}(t')^T \boldsymbol{\Sigma}(t', t) ds' dt', \quad (3.1)$$

which respectively generalize the scalar functions $\Sigma(s, t)$ and $\Gamma(s, t)$ in Section 2.1. Here $\boldsymbol{\Sigma}(s, t)$ is the matrix of covariance functions of $\mathbf{X}(t)$. Let $\boldsymbol{\alpha}_k(t) = (\alpha_{k1}(t), \dots, \alpha_{kp}(t))^T$, $k \geq 1$, denote eigenfunctions of the following generalized eigenvalue problem:

$$\begin{aligned} \max_{\boldsymbol{\alpha}(t)} \int_0^1 \int_0^1 \boldsymbol{\alpha}(s)^T \boldsymbol{\Gamma}(s, t) \boldsymbol{\alpha}(t) ds dt, \quad \text{subject to} \int_0^1 \int_0^1 \boldsymbol{\alpha}(s)^T \boldsymbol{\Sigma}(s, t) \boldsymbol{\alpha}(t) ds dt = 1 \\ \text{and } \int_0^1 \int_0^1 \boldsymbol{\alpha}_{k'}(s)^T \boldsymbol{\Sigma}(s, t) \boldsymbol{\alpha}(t) ds dt = 0, \quad 1 \leq k' \leq k-1, \end{aligned} \quad (3.2)$$

and define the m -dimensional vectors $\mathbf{w}_k = \int_0^1 \int_0^1 \mathbb{B}(t)^T \boldsymbol{\Sigma}(s, t) \boldsymbol{\alpha}_k(s) ds dt$ for $k \geq 1$. As in Theorem 2.1, we can show that $\sum_{k=1}^K \boldsymbol{\alpha}_k(t) \mathbf{w}_k^T$ is the optimal decomposition of $\mathbb{B}(t)$ in approximating the regression function and prediction.

3.2 Estimation of the optimal decomposition

Let $\mathbf{Y}_\ell = (Y_{\ell 1}, \dots, Y_{\ell m})^T$ and $\mathbf{X}_\ell(t) = (X_{\ell 1}(t), \dots, X_{\ell p}(t))^T$, $1 \leq \ell \leq n$, be n independent samples from the model (1.1). We estimate the matrices $\boldsymbol{\Sigma}(s, t)$ and $\boldsymbol{\Gamma}(s, t)$ by

$$\begin{aligned} \widehat{\boldsymbol{\Sigma}}(s, t) &= \frac{1}{n} \sum_{\ell=1}^n \{\mathbf{X}_\ell(s) - \bar{\mathbf{X}}(s)\} \{\mathbf{X}_\ell(t) - \bar{\mathbf{X}}(t)\}^T, \\ \widehat{\boldsymbol{\Gamma}}(s, t) &= \frac{1}{n^2} \left[\sum_{\ell=1}^n \{\mathbf{X}_\ell(s) - \bar{\mathbf{X}}(s)\} \{\mathbf{Y}_\ell - \bar{\mathbf{Y}}\}^T \right] \left[\sum_{\ell=1}^n \{\mathbf{Y}_\ell - \bar{\mathbf{Y}}\} \{\mathbf{X}_\ell(t) - \bar{\mathbf{X}}(t)\}^T \right] \end{aligned} \quad (3.3)$$

respectively, where $\bar{\mathbf{X}}(t) = \sum_{\ell=1}^n \mathbf{X}_\ell(t)/n$ and $\bar{\mathbf{Y}} = \sum_{\ell=1}^n \mathbf{Y}_\ell/n$. Our estimate $\hat{\boldsymbol{\alpha}}_k(t)$ is the solution to the following penalized generalized eigenvalue problem,

$$\begin{aligned} \max_{\boldsymbol{\alpha}(t)} \frac{\int_0^1 \int_0^1 \boldsymbol{\alpha}(s)^T \hat{\boldsymbol{\Gamma}}(s, t) \boldsymbol{\alpha}(t) ds dt}{\int_0^1 \int_0^1 \boldsymbol{\alpha}(s)^T \hat{\boldsymbol{\Sigma}}(s, t) \boldsymbol{\alpha}(t) ds dt + P(\boldsymbol{\alpha})}, \quad \text{subject to } \int_0^1 \int_0^1 \boldsymbol{\alpha}(s)^T \hat{\boldsymbol{\Sigma}}(s, t) \boldsymbol{\alpha}(t) ds dt = 1 \\ \text{and } \int_0^1 \int_0^1 \hat{\boldsymbol{\alpha}}_{k'}(s)^T \hat{\boldsymbol{\Sigma}}(s, t) \boldsymbol{\alpha}(t) ds dt = 0, \quad 1 \leq k' \leq k-1, \end{aligned} \quad (3.4)$$

where $P(\boldsymbol{\alpha})$ is the penalty imposed on $\boldsymbol{\alpha}(s) = (\alpha_1(s), \dots, \alpha_p(s))^T$. We provide the form of $P(\boldsymbol{\alpha})$ for the following two situations separately.

Situation 1: p is relatively small. We consider the following penalty which is a direct extension of that in (2.9):

$$P(\boldsymbol{\alpha}) = \tau \sum_{j=1}^p \|\alpha_j\|_\eta^2, \quad \text{where } \|\alpha_j\|_\eta^2 = \|\alpha_j\|_{L^2}^2 + \eta \|\alpha_j''\|_{L^2}^2. \quad (3.5)$$

Situation 2: p is relatively large. We propose a penalty that simultaneously controls the smoothness and the sparsity of $\boldsymbol{\alpha}(t)$. In Section 2.2, we have shown that $\hat{\boldsymbol{\Lambda}}(s, t)$ and $\hat{\boldsymbol{\Sigma}}(s, t)$ are consistent estimators of $\boldsymbol{\Lambda}(s, t)$ and $\boldsymbol{\Sigma}(s, t)$, respectively, when $p = 1$. This result can be extended to the case of a fixed $p > 1$ as $n \rightarrow \infty$. However, in practice, there are situations where the number p of predictor curves can be much larger than the sample size n , such as in neuroscience, the time series curves of thousands of voxels in brain can be obtained. In this case, it is more appropriate to consider the asymptotics as both $p, n \rightarrow \infty$. When both $p, n \rightarrow \infty$, although every entry of $\hat{\boldsymbol{\Lambda}}(s, t)$ and $\hat{\boldsymbol{\Sigma}}(s, t)$ converges to the corresponding entry of $\boldsymbol{\Lambda}(s, t)$ and $\boldsymbol{\Sigma}(s, t)$, respectively, for a general $\boldsymbol{\alpha}(t)$, $\int_0^1 \int_0^1 \boldsymbol{\alpha}(s)^T \hat{\boldsymbol{\Lambda}}(s, t) \boldsymbol{\alpha}(t) ds dt$ and $\int_0^1 \int_0^1 \boldsymbol{\alpha}(s)^T \hat{\boldsymbol{\Sigma}}(s, t) \boldsymbol{\alpha}(t) ds dt$ may not converge to $\int_0^1 \int_0^1 \boldsymbol{\alpha}(s)^T \boldsymbol{\Lambda}(s, t) \boldsymbol{\alpha}(t) ds dt$ and $\int_0^1 \int_0^1 \boldsymbol{\alpha}(s)^T \boldsymbol{\Sigma}(s, t) \boldsymbol{\alpha}(t) ds dt$, respectively. Inspired by the simultaneous EEG-fMRI data, where the EEG features are only related to the time series curves of a small number of voxels, we restrict our consideration to a “sparse” $\boldsymbol{\alpha}(t)$. For a scalar vector, a measurement of sparsity is its l_1 norm, and sparsity means that most of its coordinates have very small absolute values, which include the case that most coordinates are zero. We extend this concept to a vector of functions. We say $\boldsymbol{\alpha}(t) = (\alpha_1(t), \dots, \alpha_p(t))^T$ is sparse if most of the coordinate functions $\alpha_j(t)$ have very small L^2 norms. For $\boldsymbol{\alpha}(t)$, we

define two norms

$$\|\boldsymbol{\alpha}\|_{L^2,1} = \sum_{j=1}^p \|\alpha_j\|_{L^2} \quad \text{and} \quad \|\boldsymbol{\alpha}\|_{L^2,2} = \sqrt{\sum_{j=1}^p \|\alpha_j\|_{L^2}^2}, \quad (3.6)$$

where $\|\boldsymbol{\alpha}\|_{L^2,2}$ is the usual L^2 -type norm. The L^1 -type norm $\|\boldsymbol{\alpha}\|_{L^2,1}$ can measure the sparsity of $\boldsymbol{\alpha}(t)$. As an example, we consider three cases of $\boldsymbol{\alpha}(t)$ with $p = 1000$: (1). $\|\alpha_j\|_{L^2}^2 = 0.001$; (2). $\|\alpha_j\|_{L^2}^2 = c_1/j$; (3). $\|\alpha_j\|_{L^2}^2 = c_2/j^2$, where $1 \leq j \leq 1000$, and c_1 and c_2 are constants such that the L^2 -norms $\|\boldsymbol{\alpha}\|_{L^2,2}$ for the three cases are all equal to one. From Figure 3 which plots $\|\alpha_j\|_{L^2}^2$ versus j for all three cases, we observe that the third case has $\|\alpha_j\|_{L^2}$ decay the fastest and is the sparsest among all three, and the case two is sparser than the case one. The values of $\|\boldsymbol{\alpha}\|_{L^2,1}$ for these three cases are 31.62, 22.59 and 5.83, respectively, which indicates the sparseness of these vectors. Arguments

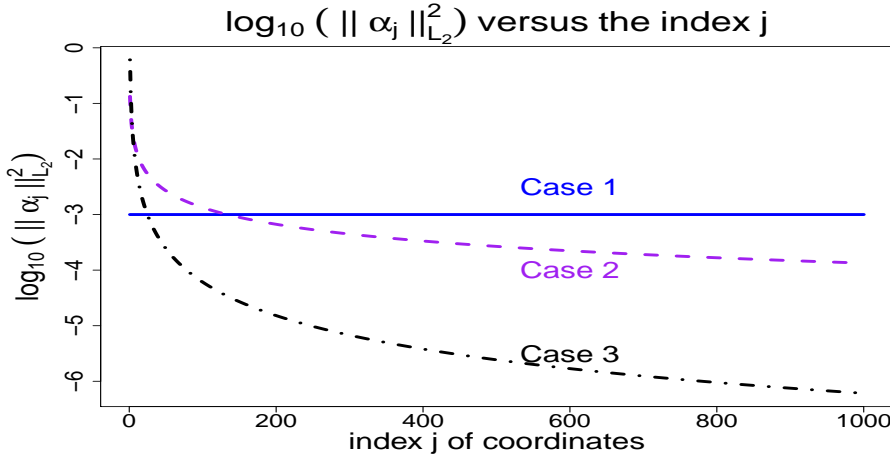


Figure 3: Plots of $\log_{10}(\|\alpha_j\|_{L^2}^2)$ versus j for the three cases: $\|\alpha_j\|_{L^2}^2 = 0.001, c_1/j, c_2/j^2$, respectively, and c_1 and c_2 are constants such that $\|\boldsymbol{\alpha}\|_{L^2,2} = 1$.

in the proof of the asymptotic result in Section 3.3 imply that if $\|\boldsymbol{\alpha}\|_{L^2,1}$ is relatively small compared to $\sqrt{n/\log p}$, $\int_0^1 \int_0^1 \boldsymbol{\alpha}(s)^T \widehat{\boldsymbol{\Lambda}}(s, t) \boldsymbol{\alpha}(t) ds dt$ and $\int_0^1 \int_0^1 \boldsymbol{\alpha}(s)^T \widehat{\boldsymbol{\Sigma}}(s, t) \boldsymbol{\alpha}(t) ds dt$ converge to $\int_0^1 \int_0^1 \boldsymbol{\alpha}(s)^T \boldsymbol{\Lambda}(s, t) \boldsymbol{\alpha}(t) ds dt$ and $\int_0^1 \int_0^1 \boldsymbol{\alpha}(s)^T \boldsymbol{\Sigma}(s, t) \boldsymbol{\alpha}(t) ds dt$, respectively. On the other hand, if we assume that $\mathbb{B}(t)$ is sparse (e.g. most of $\mathbf{b}_j(t)$'s in $\mathbb{B}(t)$ are zero), we can show that the $\boldsymbol{\alpha}_k(t)$'s in the optimal decomposition of $\mathbb{B}(t)$ have small $\|\cdot\|_{L^2,1}$ norms, where the sparsity of $\mathbb{B}(t)$ will be defined in the following Section 3.3. So we first consider to impose a Lasso-type penalty $\tau \|\boldsymbol{\alpha}\|_{L^2,1}^2$ which controls the sparsity of $\boldsymbol{\alpha}(t)$ and ensures the consistency

of our estimates. However, because $\tau\|\boldsymbol{\alpha}\|_{L^2,1}^2$ is a convex but not strictly convex function of $\boldsymbol{\alpha}$, which leads to computational difficulty in solving the optimization problem, we change $\tau\|\boldsymbol{\alpha}\|_{L^2,1}^2$ to an elasticnet-type penalty $\tau\left[(1-\lambda)\|\boldsymbol{\alpha}\|_{L^2,2}^2 + \lambda\|\boldsymbol{\alpha}\|_{L^2,1}^2\right]$ that is strictly convex. Furthermore, we control the smoothness of the coordinate functions in $\boldsymbol{\alpha}(t)$ by replacing $\|\alpha_j\|_{L^2}^2$ with $\|\alpha_j\|_\eta^2 = \|\alpha_j\|_{L^2}^2 + \eta\|\alpha_j''\|_{L^2}^2$. In summary, we propose the following simultaneous smooth-sparse penalty

$$P(\boldsymbol{\alpha}) = \tau \left\{ (1-\lambda) \left(\sum_{j=1}^p \|\alpha_j\|_\eta^2 \right) + \lambda \left(\sum_{j=1}^p \|\alpha_j\|_\eta \right)^2 \right\}, \quad (3.7)$$

where $\eta \geq 0$ controls the smoothness, $0 \leq \lambda \leq 1$ tunes the proportion of the L_1 part $\sum_{j=1}^p \|\alpha_j\|_\eta$ and the L_2 part $\sum_{j=1}^p \|\alpha_j\|_\eta^2$ in the penalty, and $\tau \geq 0$ controls the strength of the whole penalty. The τ and λ are similar to the tuning parameters in the elasticnet penalty (Zou and Hastie, 2005) for high-dimensional data analysis.

In practice, it is to be determined case-by-case regarding whether p is large. In our empirical studies, we find that there is no significant difference between the two penalties in predictive performances when $p \leq 5$, but the method with smooth penalty (3.5) is much faster than the other. When $p > 5$, significant improvement of prediction accuracy has been observed using simultaneous smooth-sparse penalty (3.7) in simulation and real data analysis.

In both of these two situations, after obtaining estimates $\hat{\boldsymbol{\alpha}}_k(t)$, $1 \leq k \leq K$, as in Section 2.2, we define new scalar predictors: $\hat{\mathbf{T}}_k = (\int_0^1 \{\mathbf{X}_1(t) - \bar{\mathbf{X}}(t)\}^T \hat{\boldsymbol{\alpha}}_k(t) dt, \dots, \int_0^1 \{\mathbf{X}_n(t) - \bar{\mathbf{X}}(t)\}^T \hat{\boldsymbol{\alpha}}_k(t) dt)^T$, and obtain the estimates $\hat{\boldsymbol{\mu}}$ and $\hat{\mathbf{w}}_k$'s using the same method as in Section 2. Finally, we estimate $\boldsymbol{\mu}_{\mathbf{Y}|\mathbf{X}}$ by $\hat{\boldsymbol{\mu}}_{\mathbf{Y}|\mathbf{X}} = \hat{\boldsymbol{\mu}} + \sum_{k=1}^K \left[\int_0^1 \{\mathbf{X}(t) - \bar{\mathbf{X}}(t)\}^T \hat{\boldsymbol{\alpha}}_k(t) dt \right] \hat{\mathbf{w}}_k$. Given a new observation $\mathbf{X}_{\text{new}}(t)$ of the functional predictors, we predict the response vector as

$$\mathbf{Y}_{\text{pred}} = \hat{\boldsymbol{\mu}} + \sum_{k=1}^K \left[\int_0^1 \{\mathbf{X}_{\text{new}}(t) - \bar{\mathbf{X}}(t)\}^T \hat{\boldsymbol{\alpha}}_k(t) dt \right] \hat{\mathbf{w}}_k. \quad (3.8)$$

3.3 Asymptotic results

We consider the asymptotic results as both the sample size n and the number p of predictive curves go to infinity, but with the dimension m of the response vector \mathbf{Y} fixed. Let

$$\mathbb{Y} = [\mathbf{Y}_1, \dots, \mathbf{Y}_n]^T, \quad \mathbb{X}(t) = [\mathbf{X}_1(t), \dots, \mathbf{X}_n(t)]^T, \quad \mathbb{E} = [\boldsymbol{\varepsilon}_1, \dots, \boldsymbol{\varepsilon}_n]^T$$

be the $n \times m$ response matrix, the $n \times p$ matrix of functional predictors and the $n \times m$ noise matrix, respectively. The sample version of model (1.1) can be written as

$$\mathbb{Y} = \mathbb{F} + \mathbb{E}, \quad \text{where} \quad \mathbb{F} = \mathbf{1}_n \boldsymbol{\mu}^T + \int_0^1 \mathbb{X}(t) \mathbb{B}(t) dt \quad (3.9)$$

is the $n \times m$ data matrix of regression function, and $\mathbf{1}_n$ is the n -dimensional vector of 1's. We estimate \mathbb{F} as

$$\widehat{\mathbb{F}} = \mathbf{1}_n \widehat{\boldsymbol{\mu}}^T + \sum_{k=1}^K \left[\int_0^1 \{ \mathbb{X}(t) - \mathbf{1}_n \bar{\mathbb{X}}(t)^T \} \widehat{\boldsymbol{\alpha}}_k(t) dt \right] \widehat{\mathbf{w}}_k^T. \quad (3.10)$$

We will provide a convergence rate for the estimation error $\|\widehat{\mathbb{F}} - \mathbb{F}\|_F$, where $\|\cdot\|_F$ is the Frobenius norm. Moreover, for a new observation $(\mathbf{X}_{\text{new}}(t), \mathbf{Y}_{\text{new}})$, we will provide a convergence rate for the prediction error $\|\mathbf{Y}_{\text{pred}} - \mathbf{Y}_{\text{new}}\|_2$, where \mathbf{Y}_{pred} is given in (3.8). We provide two regularity conditions.

(C1). For any integer $l \geq 2$,

$$E[\|\boldsymbol{\varepsilon}\|_2^{2l}] \leq l! 2^{l-1} (\sigma_\epsilon^2)^l, \quad \max_{0 \leq t \leq 1} \max_{1 \leq j \leq p} E[X_j(t)^{2l}] \leq l! 2^{l-1},$$

where σ_ϵ^2 is the sum of the variances of all coordinates of $\boldsymbol{\varepsilon}$.

The first inequality in (C1) holds for any multivariate normal distribution and σ_ϵ^2 is a measure of the noise level. The second inequality in (C1) holds if $X_j(t)$ is a Gaussian process with variance not larger than one for any $1 \leq j \leq p$ and $0 \leq t \leq 1$. If the variance of the Gaussian process $X_j(t)$ is greater than one at some time points, we can scale $X_j(t)$ to have variance not larger than one and correspondingly scale $\mathbb{B}(t)$ to keep the model unchanged, and our main results still hold for the scaled $X_j(t)$'s and $\mathbb{B}(t)$. For the coefficient matrix $\mathbb{B}(t) = [\mathbf{b}_1(t), \dots, \mathbf{b}_p(t)]^T$, we define an L_1 type norm

$$\|\mathbb{B}\|_{L^2,1} = \sum_{j=1}^p \|\mathbf{b}_j\|_{L^2,2} = \sum_{j=1}^p \sqrt{\sum_{i=1}^m \|b_{ji}\|_{L^2}^2}, \quad (3.11)$$

which measures the sparsity of $\{\mathbf{b}_1(t), \dots, \mathbf{b}_p(t)\}$.

$$(C2). \quad \lim_{n \rightarrow \infty} \sqrt{\frac{\log p}{n}} = 0 \quad \text{and} \quad \lim_{n \rightarrow \infty} \left(\sigma_\epsilon^2 + \|\mathbb{B}\|_{L^2,1}^2 \right) \sqrt{\frac{\log p}{n}} = 0.$$

This condition implies that p can be much larger than n , but should increase slower than e^n . Both the noise level σ_ϵ^2 and the sparsity of coefficient functions, $\|\mathbb{B}\|_{L^2,1}^2$, should increase slower than $\sqrt{n/\log p}$.

By Theorem 2.1, we only need the first few components with relatively large σ_k^2 . Let

$$K = \max \left\{ k : \sigma_k^2 \geq \delta (\sigma_\epsilon^2 + \|\mathbb{B}\|_{L^2,1}^2) \sqrt{\frac{\log p}{n}} \right\} \quad (3.12)$$

for a constant δ not depending on n .

Theorem 3.1. *Assume that conditions (C1) and (C2) hold, and K is chosen based on (3.12) with δ large enough. Assume that the tuning parameters satisfy*

$$\tau = M \sqrt{\frac{\log p}{n}}, \quad \lambda_0 \leq \lambda \leq 1, \quad 0 \leq \eta \leq \min_{1 \leq k \leq K} \{ \|\alpha_k\|_{L^2,1}^2 / \|\alpha_k''\|_{L^2,1}^2 \}, \quad (3.13)$$

where $0 < \lambda_0 < 1$ is a constant and M is a constant large enough. Both λ_0 and M do not depend on n . Suppose that there exists a constant $c_1 > 0$ not depending on n , such that

$$\frac{\sigma_k^2 - \sigma_{k+1}^2}{\sigma_k^2} \geq c_1, \quad \text{for all } n \text{ and } 1 \leq k \leq K. \quad (3.14)$$

Then for any $n \geq 1$, there exists an event Ω_n with $P(\Omega_n) \geq 1 - 12p^{-1}$, such that in Ω_n , we have

$$\frac{1}{n} \|\widehat{\mathbb{F}} - \mathbb{F}\|_F^2 \leq D_1 (\sigma_\epsilon^2 + \|\mathbb{B}\|_{L^2,1}^2) \sqrt{\frac{\log p}{n}}, \quad (3.15)$$

$$\mathbb{E} [\|\mathbf{Y}_{\text{pred}} - \mathbf{Y}_{\text{new}}\|_2^2 | \mathbb{X}, \mathbb{Y}] \leq D_2 (\sigma_\epsilon^2 + \|\mathbb{B}\|_{L^2,1}^2) \sqrt{\frac{\log p}{n}}, \quad (3.16)$$

where D_1 and D_2 are constants not depending on n .

The constant λ_0 can be any value between 0 and 1. Therefore, the choice of the tuning parameter λ is arbitrary as long as it is bounded away from zero and does not affect the convergence rates of the upper bounds in (3.15) and (3.16). These convergence rates imply that lower noise levels and sparser functional coefficient matrix can lead to better estimation and prediction accuracy for our method.

4 Computational issues

To solve the optimization problem (3.4), we represent each function in $\boldsymbol{\alpha}(t)$ using B-spline basis expansion, and transform (3.4) to a generalized eigenvalue problem for the concatenated coefficient vectors of these basis expansions. The number of basis functions does not affect the estimation as long as it is large enough due to the smoothness penalty. Details for solving (3.4) are given in Section S.2 in supplementary material. As in FPLS and FPCA, it is important to choose appropriate number K of components. Different ways of selecting K in FPCA has been proposed, such as hypothesis testing (Cardot *et al.*, 2003a; Horváth and Kokoszka, 2012; Su *et al.*, 2017), bootstrapping (Hall and Vial, 2006), information criteria (Yao *et al.*, 2005a; Li *et al.*, 2013), cross-validation (Hosseini-Nasab, 2013; Krämer *et al.*, 2008; Goldsmith *et al.*, 2011) and generalize cross-validation (Cardot *et al.*, 2003b). Methods for choosing the tuning parameters include restricted maximum likelihood (Wood, 2011), generalized cross-validation (Wahba, 1990; Ruppert *et al.*, 2003; Reiss and Ogden, 2007), cross-validation (Krämer *et al.*, 2008; Goldsmith *et al.*, 2011) and so on. In this paper, we choose the optimal number of components K_{opt} and the optimal tuning parameters simultaneously based on a cross-validation procedure, which is implemented in the R package **FRegSigCom**. The details are provided in the following section.

4.1 Choice of the number of components and tuning parameters

Following Section 3.2, we consider the two situations of small p and large p separately.

Situation 1: p is small and penalty (3.5) is used. There are two tuning parameters, τ and η . We choose τ from the set $\{10^{-9}, 10^{-6}, 10^{-3}, 10^1, 10^3\}$ and η from $\{10^{-7}, 10^{-5}, 10^{-3}, 10^{-1}, 10\}$. The optimal pair (τ_{opt}, η_{opt}) is chosen from the 25 pairs $\{(\tau_i, \eta_j) : 1 \leq i \leq 5, 1 \leq j \leq 5\}$, together with the optimal number K_{opt} of components, by a cross-validation procedure, where τ_i 's and η_j 's are the values in the two candidate sets for τ and η , respectively. To provide a range for K_{opt} , we notice that Theorem 2.1 suggests to select the components with relatively large values of σ_k^2 which can be estimated by the maximum value $\hat{\sigma}_k^2$ of the optimization problem (3.4). Moreover, by Theorem 2.1, the number of components cannot

exceed the dimension m of the response vector. So we propose an upper bound for K_{opt} as

$$K_{\text{upper}} = \min \left\{ k > 1 : \frac{\widehat{\sigma}_k^2}{\widehat{\sigma}_1^2 + \dots + \widehat{\sigma}_k^2} \leq 0.001 \right\} \wedge m, \quad (4.1)$$

where $a \wedge b$ denotes the smaller value of a and b . The optimal number K_{opt} of components is chosen from $\{1, \dots, K_{\text{upper}}\}$, together with $(\tau_{\text{opt}}, \eta_{\text{opt}})$ using the following algorithm.

Step 1. For each pair (τ_i, η_j) , $1 \leq i \leq 5$ and $1 \leq j \leq 5$, we calculate the upper bound $K_{\text{upper}}^{(i,j)}$ using the whole data set and (4.1).

Step 2. We randomly split the whole data set into five subsets with roughly equal sizes. For each $v \in \{1, \dots, 5\}$, let $(\mathbb{Y}^{(v)}, \mathbb{X}^{(v)}(t))$ denote the v -th subset which is used as the v -th validation set, and all other observations as the v -th training set. For each $v \in \{1, \dots, 5\}$ and each candidate pair of tuning parameters (τ_i, η_j) ,

(a). We calculate $\widehat{\boldsymbol{\alpha}}_k^{(v,i,j)}(t)$, $\widehat{\boldsymbol{\mu}}^{(v,i,j)}$ and $\mathbf{w}_k^{(v,i,j)}$ for all $k \in \{1, \dots, K_{\text{upper}}^{(i,j)}\}$, using the v -th training set.

(b). For each $k \in \{1, \dots, K_{\text{upper}}^{(i,j)}\}$, we compute

$$\widehat{\mathbb{B}}^{(v,i,j,k)}(t) = \widehat{\boldsymbol{\alpha}}_1^{(v,i,j)}(t) \widehat{\mathbf{w}}_1^{(v,i,j)T} + \dots + \widehat{\boldsymbol{\alpha}}_k^{(v,i,j)}(t) \widehat{\mathbf{w}}_k^{(v,i,j)T}$$

and the predicted responses $\mathbb{Y}_{\text{pred}}^{(v,i,j,k)} = \mathbf{1}_{n_v} \widehat{\boldsymbol{\mu}}^{(v,i,j)T} + \int_0^1 \mathbb{X}^{(v)}(t) \widehat{\mathbb{B}}^{(v,i,j,k)}(t) dt$ for the v -th validation data set, where n_v is the number of the observations in the v -th validation set. Then we calculate the validation error $e_{v,i,j,k} = \|\mathbb{Y}_{\text{pred}}^{(v,i,j,k)} - \mathbb{Y}^{(v)}\|_F^2$.

We repeat Steps (a)-(b) for all $1 \leq v \leq 5$, $1 \leq i \leq 5$ and $1 \leq j \leq 5$.

Step 3. We compute the total validation error, $e_{i,j,k}^{(\text{total})} = \sum_{v=1}^5 e_{v,i,j,k}$, for all i, j, k . Let $e_{i_0, j_0, k_0}^{(\text{total})} = \min\{e_{i,j,k}^{(\text{total})} : 1 \leq i \leq 5, 1 \leq j \leq 5, 1 \leq k \leq K_{\text{upper}}^{(i,j)}\}$. Our optimal tuning parameters are $\tau_{\text{opt}} = \tau_{i_0}$, $\eta_{\text{opt}} = \eta_{j_0}$, and $\widehat{K}_{\text{opt}} = k_0$.

Situation 2: p is large, and penalty (3.7) is used. We use the same cross-validation procedure as above except that there are three tuning parameters, τ , λ and η , in penalty (3.7). In general, people choose the three tuning parameters in a three-dimensional grid to explore various combinations of them. However, as the penalty (3.7) involves the L^1 type norm and may be applied to data with hundreds or thousands predictor curves, it will be much more

complicated and time-consuming than the first situation. To improve the computational efficiency of our algorithm for a large p , we reduce the number of candidate values for the triple parameters. In penalty (3.7), the term $\left(\sum_{j=1}^p \|\alpha_j\|_\eta\right)^2$ plays the main role for curve selection and is tuned by $\tau\lambda$. So instead of exploring all possible pairs of (τ, λ) in a two-dimensional grid, we select them from the set $\{(10^{-1}, 0.1), (1, 0.2), (10, 0.3), (100, 0.4)\}$, where the values of the multiplication $\tau\lambda$ spread over a wide range. The smoothness tuning parameter η is chosen from $\{10^{-6}, 10^{-3}, 1\}$. So the optimal triple $(\tau_{\text{opt}}, \lambda_{\text{opt}}, \eta_{\text{opt}})$ is chosen from $4 \times 3 = 12$ triple values.

5 Simulation studies

We conduct simulation studies for $p = 1$ and $p > 1$ separately. For each simulation, the intercept μ is an m -dimensional vector with all coordinates equal to one, and the noise vector $\varepsilon = (\varepsilon_1, \dots, \varepsilon_m)$, where ε_k 's are independent random variables from the same distribution $N(0, \sigma^2)$. We consider three noise levels, $\sigma = 0.01, 0.1, 1$ and three values of dimension m , $m = 1, 5, 10$. Because the wavelet-based methods conduct the fast wavelet transformation which requires the number of the observation time points to be a power of two, in all the simulations, the predictive curves are all observed at 64 equally spaced points in $[0, 1]$.

5.1 Simulations with one predictor curve

We compare our method (*new.Sm*, implemented in the R package **FRegSigCom**) to the following methods. The penalized functional regression (*pfr*, Goldsmith *et al.* (2011)) expands the sample predictor curves using the principal component basis and the coefficient function using spline basis, and is implemented in the R package **refund**. The functional regression using basis representation (*fbasis*, Ramsay and Silverman (2005) and Frbrero-Bande *et al.* (2012)) expands both the predictor curves and the coefficient function using spline basis, and is implemented in the R package **fda.usc**. The functional regression using principal components analysis (*fpcr*, Cardot *et al.* (1999)) expands both the predictor curves and the unknown coefficient function using the principal component basis, and is implemented in the R package **fda.usc**. The functional penalized PLS regression with scalar response (*fpls*,

Preda and Saporta (2005) and Krämer *et al.* (2008)) expands both the predictor curves and the unknown coefficient function using the FPLS basis, and is implemented in the R package **fda.usc**. The functional regression using nonparametric kernel estimation (*fnp*, Ferraty and Vieu (2006b)) is implemented in the R package **fda.usc**. The Gaussian process regression for multivariate scalar-on-function regression (*gp-msof*, Wang *et al.* (2017)) conducts PCA on the multivariate response and then fits a nonparametric model for each PC score using the Gaussian process regression (O'Hagan and Kingman, 1978; Rasmussen and Williams, 2006). The code for *gp-msof* is provided by the authors of Wang *et al.* (2017). Two wavelet based methods, *wLasso* (Zhao *et al.*, 2012) and *wwLasso* (Zhao *et al.*, 2015), first transform the predictor curves to the wavelet coefficient vectors using the fast wavelet transformation, and then apply Lasso or weighted Lasso to the wavelet coefficients. We use the R package **wavethresh** to perform the fast wavelet transformation and the R package **glmnet** to perform Lasso and weighted Lasso. In *new.Sm*, *pfr* and *fbasis*, the numbers of B-spline basis functions is chosen to be the same and equal to 30 for all simulations and real data analysis. For *fbasis*, *fpcr* and *fpls*, we choose the smooth tuning parameter from the set $\{10^{-10}, 10^{-9}, 10^{-8}, \dots, 1, 10, \dots, 10^9, 10^{10}\}$, which leads to better performance than the default settings. In *wLasso*, we choose the option `family="mgaussian"` in function `cv.glmnet` to jointly fit the multivariate response by Lasso. However, in *wwLasso*, if we choose the option `family="mgaussian"`, the prediction error will greatly increase, so we fit each coordinate of the response separately.

We perform two sets of simulations with different ways to generate the predictor curves and coefficient functions.

Simulation 1. $X(t)$ is generated from a Gaussian process with covariance function $\exp\{-[30(t-t')]^2\}$. The coefficient $\mathbf{b}(t) = (b_1(t), \dots, b_m(t))^T$ is given by $b_k(t) = \sin(3\pi t + k) + \cos(3\pi t + k)$, $1 \leq k \leq m$.

Simulation 2. $X(t)$ is generated by the basis expansion, $X(t) = \sum_{k=1}^{20} [V_{k1} \sin(2k\pi t) + V_{k2} \cos(2k\pi t)]$, where $V_{kj} \sim N(0, 1/k^{1/2})$ for $1 \leq k \leq 20$ and $j = 1, 2$ are independent. The coefficient $\mathbf{b}(t) = \mathbb{M}\boldsymbol{\beta}(t)$, where \mathbb{M} is an $m \times 3$ matrix with each entry independently generated from the uniform distribution in $(0, 1)$, $\boldsymbol{\beta}(t) = (\beta_1(t), \beta_2(t), \beta_3(t))^T$, with $\beta_1(t) = \cos(2\pi t)$, $\beta_2(t) = 2t^2$ and $\beta_3(t) = 1/(1+t)$.

Sample curves of $X(t)$ in these two simulations are plotted in Figure S.1 of supplementary material. We generate data from the model $\mathbf{Y} = \boldsymbol{\mu} + c \int_0^1 X(t) \mathbf{b}(t) dt + \boldsymbol{\varepsilon}$, where c is a scaling constant such that when the noise level $\sigma = 1$, the signal-to-noise ratio is equal to 1. For each setting, we repeat the following procedure 100 times. In each repeat, we generate a training data of size 100 and a test data set $\{X_{\text{test},\ell}(t), \mathbf{Y}_{\text{test},\ell} : 1 \leq \ell \leq 500\}$ of size 500. We use the training set to select tuning parameters and fit model, and apply the fitted model to the test data to calculate the mean squared prediction error (MSPE)

$$\text{MSPE} = \frac{1}{500} \frac{\sum_{\ell=1}^{500} \|\widehat{\mathbf{Y}}_{\ell}^{\text{pred}} - \mathbf{F}_{\text{test},\ell}\|_2^2}{m},$$

for each method, where $\widehat{\mathbf{Y}}_{\ell}^{\text{pred}}$ is the predicted response vector for $X_{\text{test},\ell}(t)$ and $\mathbf{F}_{\text{test},\ell} = \boldsymbol{\mu} + \int_0^1 X_{\text{test},\ell}(t) \mathbf{b}(t) dt$. The averages and standard deviations of the MSPEs from 100 replicates for Simulations 1 and 2 are summarized in Table 1 which show some interesting patterns.

(1). When the noise level is relatively small ($\sigma = 0.01, 0.1$), our method has a large advantage over other methods, especially when m is relatively large. For example, when $m = 10$ and $\sigma = 0.01$, the averaged MSPEs of other methods are at least 24 times higher than that of our method in Simulation 1, and 6.3 times higher in Simulation 2.

(2). When the noise level is relatively large ($\sigma = 1$), for $m = 1$, our method, *pfr* and *fbasis* have close MSPEs which are lower than others in both simulations; when $m > 1$, our method has the best predictive performance.

(3). The MSPEs of our method decrease when m increases in both simulations for all noise levels. In Simulation 2, for any m , the coordinates of the response have the same distribution which is also the same as that for $m = 1$. So when $m > 1$, if we separately fit the model for each coordinate of the response, the MSPEs should be the same as those of $m = 1$. By taking care of the correlation structure in response, our method has improved predictive accuracy when m is larger. In Simulation 2, for $\sigma = 0.1$, the averaged number of components chosen by our method is 3.34 for $m = 5$ and 3.26 for $m = 10$. Compared to the case of $m = 5$, despite there are more coordinates when $m = 10$, our method chooses less components. So our method makes more aggressive dimension reduction when $m = 10$ than when $m = 5$, which leads to improvement of prediction accuracy. Similarly we can explain the pattern in Simulation 1.

Table 1: The averages and standard deviations (in parenthesis) of MSPEs in Simulations 1 and 2.

Simulation 1						
σ	m	<i>new.Sm</i>	<i>pfr</i>	<i>fbasis</i>	<i>fpcr</i>	<i>fpls</i>
0.01	1	$0.28(0.11) \times 10^{-4}$	$5.3(3.8) \times 10^{-4}$	$3.6(0.9) \times 10^{-4}$	0.34(0.16)	$0.002(0.0003)$
	5	$0.14(0.04) \times 10^{-4}$	$4.2(1.6) \times 10^{-4}$	$2.3(0.4) \times 10^{-4}$	0.30(0.10)	$0.001(0.0002)$
	10	$0.09(0.02) \times 10^{-4}$	$4.0(1.4) \times 10^{-4}$	$2.2(0.4) \times 10^{-4}$	0.31(0.11)	$0.001(0.0002)$
0.1	1	$1.8(0.7) \times 10^{-3}$	$4.9(0.8) \times 10^{-3}$	$4.0(1.0) \times 10^{-3}$	0.37(0.16)	$2.8(0.6) \times 10^{-3}$
	5	$0.9(0.3) \times 10^{-3}$	$3.4(0.4) \times 10^{-3}$	$3.0(0.4) \times 10^{-3}$	0.30(0.11)	$2.2(0.3) \times 10^{-3}$
	10	$0.6(0.1) \times 10^{-3}$	$3.4(0.3) \times 10^{-3}$	$3.0(0.3) \times 10^{-3}$	0.31(0.12)	$2.1(0.3) \times 10^{-3}$
1	1	0.10(0.05)	0.09(0.04)	0.10(0.05)	0.49(0.20)	0.23(0.08)
	5	0.07(0.03)	0.08(0.02)	0.10(0.03)	0.43(0.11)	0.20(0.04)
	10	0.05(0.02)	0.09(0.02)	0.10(0.02)	0.46(0.11)	0.21(0.04)
σ	m	<i>fnp</i>	<i>gp-msof</i>	<i>wLasso</i>	<i>wwLasso</i>	
0.01	1	0.90(0.04)	0.99(0.03)	0.002(0.0003)	0.002(0.0004)	
	5	0.89(0.03)	1.02(0.02)	0.002(0.0002)	0.002(0.0003)	
	10	0.90(0.03)	1.02(0.02)	0.002(0.0002)	0.001(0.0002)	
0.1	1	0.91(0.04)	1.02(0.02)	$6.3(1.9) \times 10^{-3}$	$5.1(1.3) \times 10^{-3}$	
	5	0.90(0.03)	1.02(0.02)	$4.1(0.8) \times 10^{-3}$	$4.7(0.5) \times 10^{-3}$	
	10	0.90(0.03)	1.02(0.02)	$3.6(0.5) \times 10^{-3}$	$4.6(0.4) \times 10^{-3}$	
1	1	0.92(0.05)	1.00(0.03)	0.39(0.12)	0.32(0.09)	
	5	0.92(0.03)	1.02(0.02)	0.25(0.05)	0.31(0.04)	
	10	0.92(0.03)	1.02(0.02)	0.21(0.04)	0.31(0.02)	
Simulation 2						
σ	m	<i>new.Sm</i>	<i>pfr</i>	<i>fbasis</i>	<i>fpcr</i>	<i>fpls</i>
0.01	1	$1.8(0.7) \times 10^{-5}$	$2.3(2.7) \times 10^{-3}$	$6.8(2.7) \times 10^{-5}$	0.13(0.08)	0.014(0.011)
	5	$1.4(0.3) \times 10^{-5}$	$1.9(0.5) \times 10^{-3}$	$6.3(0.9) \times 10^{-5}$	0.12(0.05)	0.011(0.002)
	10	$1.0(0.2) \times 10^{-5}$	$1.8(0.4) \times 10^{-3}$	$6.3(0.6) \times 10^{-5}$	0.11(0.05)	0.011(0.002)
0.1	1	$1.3(0.6) \times 10^{-3}$	$6.9(0.4) \times 10^{-3}$	$3.7(1.2) \times 10^{-3}$	0.13(0.07)	0.015(0.01)
	5	$0.9(0.2) \times 10^{-3}$	$5.8(0.5) \times 10^{-3}$	$3.5(0.5) \times 10^{-3}$	0.12(0.05)	0.013(0.003)
	10	$0.8(0.2) \times 10^{-3}$	$5.8(0.8) \times 10^{-3}$	$3.6(0.4) \times 10^{-3}$	0.12(0.06)	0.013(0.002)
1	1	0.06(0.04)	0.06(0.03)	0.08(0.05)	0.59(0.24)	0.15(0.05)
	5	0.05(0.02)	0.06(0.02)	0.08(0.03)	0.59(0.13)	0.15(0.04)
	10	0.04(0.01)	0.06(0.01)	0.08(0.02)	0.59(0.11)	0.16(0.03)
σ	m	<i>fnp</i>	<i>gp-msof</i>	<i>wLasso</i>	<i>wwLasso</i>	
0.01	1	0.91(0.04)	1.01(0.03)	0.0014(0.0003)	0.0015(0.0003)	
	5	0.90(0.03)	1.01(0.02)	0.0014(0.0002)	0.0015(0.0003)	
	10	0.90(0.03)	1.00(0.02)	0.0015(0.0003)	0.0016(0.0003)	
0.1	1	0.90(0.04)	1.00(0.03)	$4.7(1.4) \times 10^{-3}$	$4.4(1.4) \times 10^{-3}$	
	5	0.90(0.04)	1.01(0.03)	$3.3(0.7) \times 10^{-3}$	$4.0(0.6) \times 10^{-3}$	
	10	0.90(0.03)	1.02(0.01)	$3.1(0.5) \times 10^{-3}$	$4.2(0.4) \times 10^{-3}$	
1	1	0.91(0.04)	1.01(0.02)	0.29(0.06)	0.22(0.05)	
	5	0.91(0.03)	1.02(0.03)	0.16(0.04)	0.20(0.03)	
	10	0.92(0.04)	1.02(0.03)	0.14(0.03)	0.21(0.02)	

(4). Our method, *fpls* and *fPCA* all consider decompositions of the coefficient functions. The *fpcr* only uses $X(t)$ to construct the component functions and ignores information in \mathbf{Y} . The *fpls* and our method use information in both $X(t)$ and \mathbf{Y} , but our method estimates the optimal decomposition for prediction. So our method outperforms *fpls*, which is better than *fPCA*, in these simulations.

(5). When $\sigma = 0.1$, the two wavelet based methods have similar performance with *pfr* and *fbasis*. As m increases, *wLasso* has decreased prediction error as the multivariate response is jointly fitted and the correlation structure in response has been taken into account.

(6). All the data in these simulations are generated from linear model. But *fnp* is a nonparametric method which is not specialized for linear model. The high MSPEs of *fnp* may be due to its complication. So does the *gp-msof* which also uses nonparametric method.

5.2 Simulations with multiple predictor curves

When p is moderate or large, many methods in Simulations 1 and 2 are not computationally feasible. We compare our methods, *new.SmSp* with the simultaneous smooth-sparse penalty in (3.7) and *new.Sm* with the smooth only penalty in (3.5), with *wLasso* and *wwLasso*. In addition, we consider two more hybrid methods *FPCA+gSCAD* (Lian, 2013; Kong *et al.*, 2016b) and *FPCA+gLasso* (Zhu and Cox, 2009), which perform FPCA on each functional predictor using the R package `fda`, and then use the PC scores as new scalar predictors to fit penalized regression model with the R package `grpreg` by imposing the group SCAD or group Lasso penalty, respectively. The number of components in FPCA is chosen by the criterion of 99% variations explained. But these two FPCA based methods are not computationally feasible for large p , such as 1000.

We generate the predictor curves and coefficient functions in the following two different ways.

Simulation 3. We take $p = 50$.

(1). $\mathbf{X}(t) = (X_1(t), \dots, X_{50}(t))^T$ is generated by basis expansion

$$X_j(t) = \sum_{k=1}^{20} [V_{k1}^{(j)} \sin(2k\pi t) + V_{k2}^{(j)} \cos(2k\pi t)], \quad 1 \leq j \leq p,$$

where $\mathbf{V}_{ki} = (V_{ki}^{(1)}, \dots, V_{ki}^{(50)})^T$ has a multivariate normal distribution with mean zero and covariance matrix with diagonal entries equal to $1/\sqrt{k}$ and off-diagonal entries equal to ρ/\sqrt{k} , for $1 \leq k \leq 20$ and $i = 1, 2$. The \mathbf{V}_{ki} 's are independent. The value $0 \leq \rho \leq 1$ controls the correlation between $X_j(t)$'s. The larger is ρ , the stronger is the correlation. We consider two values $\rho = 0.2, 0.7$.

(2). The coefficient $\mathbb{B}(t) = [\boldsymbol{\beta}_1(t), \boldsymbol{\beta}_2(t), \boldsymbol{\beta}_3(t)] \mathbb{M}$ is a $p \times m$ matrix, where \mathbb{M} is a $3 \times m$ matrix with each entry independently generated from the uniform distribution in $(0, 1)$. For $1 \leq k \leq 3$, $\boldsymbol{\beta}_k(t) = (\beta_{1k}(t), \dots, \beta_{pk}(t))^T$ is a p -dimensional vector with $\beta_{1k}(t) = t^k$, $\beta_{2k}(t) = \cos(k\pi t)$, $\beta_{3k}(t) = 1/(t+k)$, $\beta_{4k}(t) = \log(t+k)$, $\beta_{5k}(t) = e^{-kt^2}$, and $\beta_{jk}(t) = 0$ if $j > 5$. So only the first five predictor curves have nonzero coefficients and are viewed as true features.

Simulation 4. We take $p = 1000$.

(1). To generate $\mathbf{X}(t) = (X_1(t), \dots, X_{1000}(t))^T$, we first generate independent curves $W_j(t)$'s from a Gaussian processes with covariance function $\exp\{-[30(t-t')]^2\}$, $1 \leq j \leq 1000 + Lag$, and let $X_j(t) = [W_{j+1}(t) + \dots + W_{j+Lag}(t)]/\sqrt{Lag}$, where Lag is a positive integer used to control the correlation between $X_j(t)$'s. A larger Lag leads to stronger correlation between $X_j(t)$'s. We take $Lag = 2, 5$.

(2). The coefficient $\mathbb{B}(t) = [\boldsymbol{\beta}_1(t), \boldsymbol{\beta}_2(t), \boldsymbol{\beta}_3(t)] \mathbb{M}$ is a $p \times m$ matrix, where \mathbb{M} is defined in the same way as in Simulation 3. For $1 \leq k \leq 3$, $\boldsymbol{\beta}_k(t) = (\beta_{1k}(t), \dots, \beta_{pk}(t))^T$ is a p -dimensional vector with $\beta_{1,k}(t) = 2(t+1)e^{-kt}$, $\beta_{11,k}(t) = \sin(k\pi t/2)/\sqrt{1+t}$, $\beta_{21,k}(t) = 3 \sinh(-t)/k + t^2$, $\beta_{31,k}(t) = 0.5(1+t)^k \cos(k\pi t)$, $\beta_{41,k}(t) = \tan(t)/(1+kt^2)$ and $\beta_{jk}(t) = 0$ for all other j 's. So only the five predictor curves, $X_1(t), X_{11}(t), X_{21}(t), X_{31}(t), X_{41}(t)$, have nonzero coefficients and are viewed as true features.

We generate data from model $\mathbf{Y}_\ell = \mathbf{F}_\ell + \boldsymbol{\varepsilon}_\ell$, where $\mathbf{F}_\ell = \boldsymbol{\mu} + c \int_0^1 \mathbf{X}_\ell(t)^T \mathbb{B}(t) dt$, $1 \leq \ell \leq 100$, and c is a scaling factor such that when the noise level $\sigma = 1$, the signal-to-noise ratio is equal to 1. We conduct similar procedure as in Section 5.1 by performing 100 replications, where each replicate has training data of size 100 and test data of size 500. The averages and standard deviations of the MSPEs from 100 replicates are summarized in Table 2. In both simulations, our method *new.SmSp* has the lowest MSPEs. The introduction of the simultaneous smooth-sparse penalty greatly improves the performance of our method

compared to that without sparsity penalty. With the increase of m , the MSPEs of our method *new.SmSp* decreases, especially when $\sigma = 1$.

In addition, we calculate the sensitivity and specificity of each method for curve selection. Let $\widehat{\mathbb{B}}(t) = [\widehat{\mathbf{b}}_1(t), \dots, \widehat{\mathbf{b}}_p(t)]^T$ be the estimate of the coefficient $\mathbb{B}(t) = [\mathbf{b}_1(t), \dots, \mathbf{b}_p(t)]^T$, where $\mathbf{b}_j(t)$ is the coefficient of the j -th predictor curve, $1 \leq j \leq p$. Sensitivity and specificity are respectively defined as

$$\text{sensitivity} = \frac{\text{the number of } j\text{'s with both } \mathbf{b}_j(t) \neq \mathbf{0} \text{ and } \widehat{\mathbf{b}}_j(t) \neq \mathbf{0}}{\text{the number of } j\text{'s with } \mathbf{b}_j(t) \neq \mathbf{0}}$$

and

$$\text{specificity} = \frac{\text{the number of } j\text{'s with both } \mathbf{b}_j(t) = \mathbf{0} \text{ and } \widehat{\mathbf{b}}_j(t) = \mathbf{0}}{\text{the number of } j\text{'s with } \mathbf{b}_j(t) = \mathbf{0}}.$$

Tables S.1 and S.2 of supplementary material summarize the sensitivity and specificity of each method. The method *new.Sm* has sensitivity equal 1 and specificity equal 0 because it does not do variable selection and includes all variables in model fitting. Our method *new.SmSp* has the highest sensitivity and lower specificity than wavelet-based methods or FPC-based methods. That implies that *new.SmSp* selects more curves than other methods, including both true feature curves and non-feature curves.

6 Applications

We consider two data sets: the corn data with single predictor curve and the simultaneous EEG-fMRI data with a large number of predictor curves.

6.1 Corn data

This data set consists of 80 samples of corn, and is available at Eigenvector Research (<http://www.eigenvector.com/data/Corn/index.html>). The moisture, oil, protein and starch values of each corn sample are measured together with its NIR spectrum curve with wavelength range from 1100nm to 2498nm at every 2 nm.

Table 2: The averages (and standard deviations) of MSPEs in Simulations 3 and 4.

Simulation 3								
ρ	σ	m	<i>new.SmSp</i>	<i>new.Sm</i>	<i>wLasso</i>	<i>wwLasso</i>	<i>FPCA+gSCAD</i>	<i>FPCA+gLasso</i>
0.2	0.01	1	0.050(0.026)	0.349(0.165)	0.375(0.156)	0.186(0.073)	0.605(0.135)	0.628(0.121)
		5	0.049(0.015)	0.364(0.093)	0.308(0.094)	0.184(0.051)	0.602(0.099)	0.625(0.096)
		10	0.049(0.013)	0.360(0.075)	0.300(0.088)	0.181(0.046)	0.599(0.083)	0.624(0.085)
	0.1	1	0.064(0.030)	0.363(0.174)	0.379(0.156)	0.198(0.088)	0.598(0.133)	0.628(0.125)
		5	0.057(0.017)	0.360(0.082)	0.316(0.092)	0.195(0.048)	0.610(0.098)	0.637(0.097)
		10	0.053(0.013)	0.364(0.084)	0.317(0.086)	0.197(0.042)	0.611(0.088)	0.628(0.093)
	1	1	0.536(0.200)	0.883(0.151)	0.893(0.155)	0.724(0.205)	0.952(0.108)	0.957(0.114)
		5	0.267(0.068)	0.687(0.104)	0.667(0.125)	0.679(0.108)	0.940(0.080)	0.940(0.082)
		10	0.228(0.045)	0.593(0.093)	0.603(0.109)	0.677(0.104)	0.941(0.060)	0.943(0.061)
0.7	0.01	1	0.051(0.022)	0.174(0.076)	0.240(0.096)	0.113(0.052)	0.360(0.103)	0.349(0.088)
		5	0.049(0.013)	0.180(0.043)	0.204(0.056)	0.106(0.028)	0.359(0.065)	0.347(0.056)
		10	0.047(0.011)	0.182(0.038)	0.207(0.045)	0.107(0.028)	0.357(0.059)	0.349(0.053)
	0.1	1	0.059(0.023)	0.191(0.081)	0.256(0.100)	0.125(0.054)	0.361(0.089)	0.357(0.086)
		5	0.054(0.013)	0.188(0.046)	0.216(0.051)	0.121(0.033)	0.368(0.059)	0.356(0.054)
		10	0.051(0.012)	0.184(0.035)	0.213(0.044)	0.121(0.030)	0.363(0.055)	0.354(0.051)
	1	1	0.436(0.153)	0.537(0.172)	0.670(0.192)	0.574(0.193)	0.733(0.142)	0.736(0.151)
		5	0.276(0.064)	0.445(0.072)	0.435(0.085)	0.537(0.098)	0.709(0.075)	0.707(0.072)
		10	0.230(0.042)	0.377(0.059)	0.385(0.063)	0.522(0.077)	0.699(0.061)	0.695(0.059)

Simulation 4								
<i>Lag</i>	σ	m	<i>new.SmSp</i>	<i>new.Sm</i>	<i>wLasso</i>	<i>wwLasso</i>		
2	0.01	1	0.187(0.109)	0.973(0.043)	0.465(0.143)	0.378(0.138)		
		5	0.174(0.066)	0.968(0.040)	0.394(0.098)	0.351(0.097)		
		10	0.148(0.042)	0.971(0.040)	0.372(0.073)	0.350(0.077)		
	0.1	1	0.207(0.120)	0.976(0.040)	0.465(0.154)	0.382(0.144)		
		5	0.163(0.062)	0.971(0.041)	0.399(0.117)	0.376(0.110)		
		10	0.171(0.052)	0.974(0.040)	0.388(0.091)	0.370(0.091)		
	1	1	0.657(0.244)	1.03(0.06)	0.884(0.160)	0.847(0.184)		
		5	0.328(0.086)	0.997(0.043)	0.632(0.131)	0.785(0.124)		
		10	0.274(0.063)	0.987(0.041)	0.572(0.095)	0.775(0.119)		
5	0.01	1	0.181(0.132)	0.953(0.052)	0.459(0.184)	0.363(0.168)		
		5	0.154(0.050)	0.843(0.052)	0.376(0.088)	0.330(0.089)		
		10	0.149(0.053)	0.944(0.050)	0.362(0.099)	0.318(0.094)		
	0.1	1	0.180(0.106)	0.945(0.052)	0.437(0.155)	0.348(0.138)		
		5	0.164(0.059)	0.947(0.053)	0.392(0.100)	0.353(0.098)		
		10	0.168(0.058)	0.954(0.055)	0.379(0.088)	0.352(0.088)		
	1	1	0.645(0.220)	1.02(0.054)	0.901(0.137)	0.848(0.166)		
		5	0.334(0.112)	0.987(0.056)	0.635(0.143)	0.772(0.130)		
		10	0.259(0.051)	0.958(0.054)	0.553(0.090)	0.737(0.114)		

People are interested in predicting the values of the four ingredients of corn based on the NIR spectrum curve. So we consider the functional linear regression model with the NIR spectrum curve as the single functional predictor and the four ingredients as the multivariate response. We plot all 80 predictor curves, together with their centered versions, in Figure 4. The four response variables are all centered and scaled to have variance one, and their histograms are shown in Figure S.2 in supplementary material.

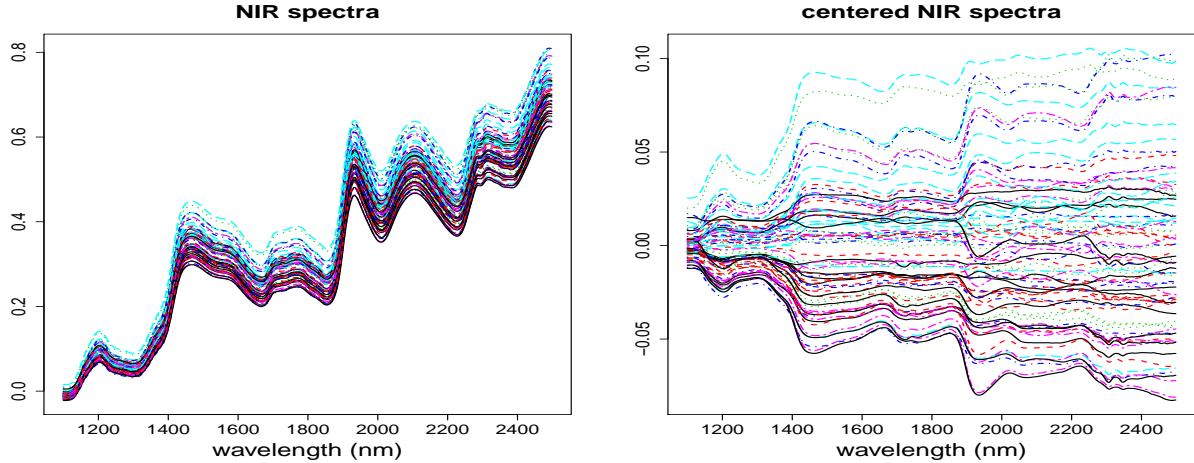


Figure 4: The original and centered NIR spectra curves of 80 samples in the corn data.

We first apply all the methods in Section 5.1 for Simulations 1 and 2 to this data set and compare their prediction performance. We perform 100 iterations, and in each iteration, we randomly split the total 80 observations into a training set with 60 observations and a test set with 20 observations. In addition to MSPE, we also calculate the R^2 to evaluate the goodness of fit of each method using the following formula in each repeat,

$$R^2 = 1 - \frac{\sum_{\ell=1}^{60} \|\hat{\mathbf{Y}}_{\text{fitted},\ell} - \mathbf{Y}_{\text{train},\ell}\|_2^2}{\sum_{\ell=1}^{60} \|\mathbf{Y}_{\text{train},\ell} - \bar{\mathbf{Y}}_{\text{train}}\|_2^2}, \quad (6.1)$$

where the four-dimensional vector $\mathbf{Y}_{\text{train},\ell}$ is the ℓ -th observation of the response in the training set, and $\hat{\mathbf{Y}}_{\text{fitted},\ell}$ is the corresponding fitted value, $1 \leq \ell \leq 60$. The average (and standard deviation) of the MSPEs over 100 repeats is 0.18 (0.03) for our method, 0.32 (0.08) for *pfr*, 0.43 (0.07) for *fbasis*, 0.34 (0.05) for *fpcr*, 0.22 (0.03) for *fpls*, 0.87 (0.14) for *fnp*, 1.01 (0.14) for *gp-msof*, 0.31 (0.06) for *wLasso* and 0.91 (0.13) for *wwLasso*. The average (and standard deviation) of the R^2 's over 100 repeats is 91% (0.8%) for our method, 78% (0.7%)

for pfr , 66% (1%) for $fbasis$, 76% (2%) for $fpcr$, 87% (1%) for $fpls$, 40% (5%) for fnp , 10% (6%) for $gp-msof$, 78% (3%) for $wLasso$ and 15% (3%) for $wwLasso$.

Given a new predictor curve, in addition to the predicted values, it is also of interest to provide prediction intervals for the response to evaluate the uncertainty of prediction. With the proposed two-step procedure, we cannot provide explicit formula for the estimates of coefficient functions and their asymptotic variance matrix. So we propose to use the bootstrap method to calculate the prediction intervals, which also accounts for the variations due to tuning parameter selection. As an example, we use all the observations except the first four as the training data, and the first four observations as the test data. Using this training data, we will calculate the bootstrap prediction interval and estimate the expectation of the mean squared prediction error for each of the first four predictor curves. Specifically, we repeat the following procedure 1000 times. In each iteration, we draw a bootstrap sample with replacement from the training data and with same size as the training data. We fit the model using the bootstrap sample and our method, and then calculate the predicted response for each observation in the test data. From the 1000 repeats, we obtain 1000 predicted values for each coordinate of the response. Using the 2.5% and 97.5% percentiles of these predicted values as the lower and upper limits, we get a 95% bootstrap prediction interval for the corresponding coordinate of the response. We show the predictor curves in the first four observations and provide the bootstrap prediction intervals in Figure S.3 and Table S.3 of supplementary material, respectively. The expected mean squared prediction error for the first four observations are estimated as 0.13, 0.24, 0.04, 0.09, respectively.

Finally, applying our method to all 80 observations, we obtain a model which is built upon four components. The ratio of the four estimators $\widehat{\sigma}_k^2$ of σ_k^2 , $1 \leq k \leq 4$, is 0.51 : 0.34 : 0.14 : 0.01. We plot the estimators $\widehat{\alpha}_k(t)$'s of the functions $\alpha_k(t)$ for the four components in Figure 5.

6.2 Simultaneous EEG-fMRI data

We consider a simultaneous EEG-fMRI data set (<https://openfmri.org>, access number ds000116) from the project “*Auditory and Visual Oddball EEG-fMRI*”. This data set contains 102 observations recorded in 102 runs, each of which lasts 340 seconds. During each

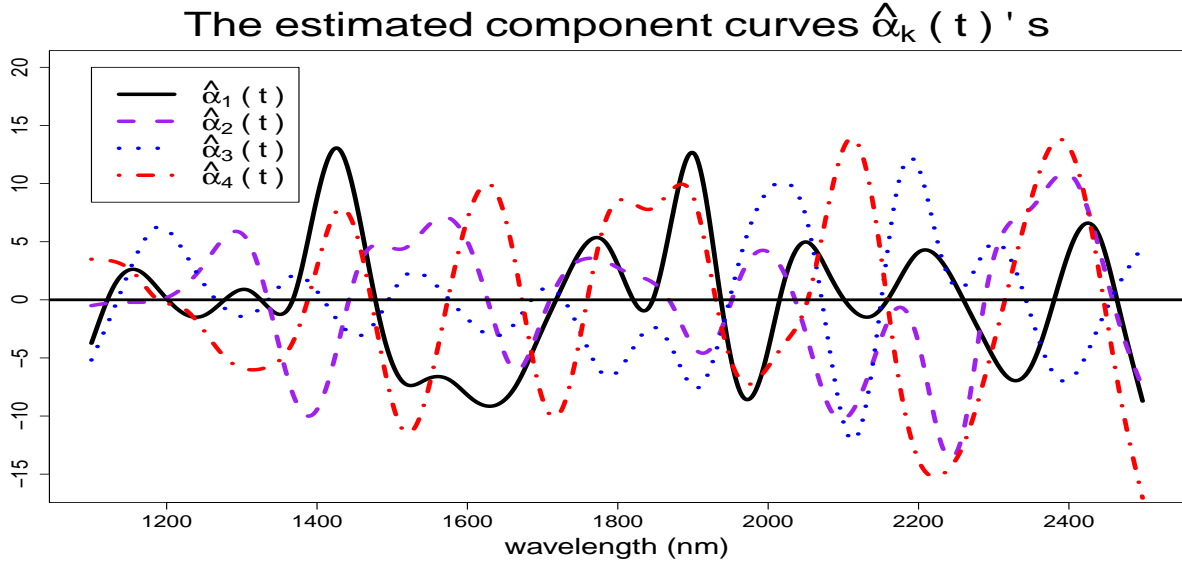


Figure 5: The estimates $\hat{\alpha}_k(t)$, $1 \leq k \leq 4$, for the corn data.

run, 125 total visual (or auditory) stimuli were presented and each of them lasts 200 ms followed by a 2 ~ 3 seconds intertrial interval. For the background and details of the experiments, we refer the reader to Walz *et al.* (2013). In each observation, both fMRI time series and EEG time series are simultaneously recorded for the subject. We will extract multivariate responses from EEG data and functional predictors from fMRI data.

The EEG data were recorded with sampling rate 1,000 Hz and has been preprocessed to remove gradient-artifact and be re-referenced to 34-channel electrode space (Walz *et al.*, 2013). So in each observation, the EEG data contains 34 times series each of which has 340,000 observation time points. It is known that the fluctuations of EEG power spectrum in different frequency bands are related to different brain activities. For example, the gamma frequency band (between 25Hz and 100Hz) is thought to be related to visual (Gray *et al.*, 1989; Engel *et al.*, 1991; Fries *et al.*, 2001; Womelsdorf *et al.*, 2006), auditory (Brosch *et al.*, 2002; Edwards *et al.*, 2005), and other sensory processing. For each observation, we calculate a gamma power spectrum using “Chronux” (Mitra Lab in Cold Spring Harbor Laboratory, 2014), a popular software package implemented as a Matlab library for the analysis of neural data. The 34 EEG time series for 34 channels are combined to calculate a gamma power spectrum for each observation. Examples of gamma power spectrum for two observations

are plotted in the top of Figure S.4 of supplementary material. There are many peaks in these spectrum curves and the numbers and positions of these peaks may vary for different observations. We identify ten common peaks and plot them in the bottom of Figure S.4 in supplementary material. We use the integral of each peak in the interval shown in Figure S.4 with length 0.2 HZ to measure its magnitude. The ten magnitude values for the ten peaks form our ten-dimensional multivariate response. As the values of the magnitudes are highly skewed distributed, we transform the responses using the function $\sqrt{\ln(1 + u)}$, and scale the transformed values such that each coordinate of the ten-dimensional response vector has sample variance one. We draw the histograms for ten coordinates of the transformed response in Figure S.5 of supplementary material.

The fMRI data contain 170 three-dimensional images obtained every 2 seconds. Each fMRI image is divided into $64 \times 64 \times 32 = 131,072$ voxels. Therefore, in each of the 102 observations, the fMRI data can be viewed as a collection of 131,072 time series curves. We process these curves in two different ways and consider two different functional regression models.

(1). Using regions of interest (ROI) curves.

We partition the brain voxels into 68 ROIs using the WFU PickAtlas Tools (Lancaster *et al.*, 1997, 2000; Maldjian *et al.*, 2003) in Matlab SPM12 (Ashburner *et al.*, 2014) based on the TD Brodmann areas of human brain (Brodmann, 1909). We average the time series curves for all voxels in each ROI and use the $p = 68$ averaged curves as functional predictors.

With 68 close to the number of functional predictors in Simulation 3, we apply all the methods used in Simulation 3 to this model. We perform 100 iterations. In each iteration, we randomly split the 102 observations into the training set with 80 observations and the test set with 22 observations. We calculate both the MSPE and the R^2 , and summarize them in Table 3. The average MSPEs of our method with and without sparsity penalty are very close, and much lower than other methods. Among the 68 ROIs, 33 of them are selected in all 100 iterations by our method (shown in Figure S.6 and listed in Table S.4 of supplementary material). The activities in those regions may be related to the fluctuations of spectrum at the ten peaks. For example, the Brodmann area (BA) 7 is the visuo-motor coordination and is involved in locating objects in space; the BA 8 includes the frontal eye

fields and is involved in planning complex movements; the BAs 17 and 18 are respectively the primary and secondary visual cortex that processes visual information; the optic tract is a part of the visual system; and the Lateral Dorsal Nucleus is a relay center in the thalamus for the visual pathway.

Table 3: The averages (and standard deviations) of MSPEs and R^2 in the first model for the simultaneous EEG-fMRI data.

	<i>new.SpSm</i>	<i>new.Sm</i>	<i>wLasso</i>	<i>wwLasso</i>	<i>FPCA+gSCAD</i>	<i>FPCA+gLasso</i>
MSPE	0.29(0.09)	0.29 (0.07)	1.02(0.16)	1.02(0.16)	1.12(1.08)	1.19(1.3)
R^2	0.86(0.03)	0.88(0.01)	0.02(0.03)	0.02(0.02)	0.03(0.03)	0.04(0.04)

(2). Using voxel curves.

In the second model, we work on the voxel time serie curves directly. With a pre-screen procedure described in Section S.3.3 in supplementary material, we select $p = 3559$ voxels and use their time series curves as our predictive curves. We show the positions of the 3559 voxels in the brain images in Figure S.7 and plot 200 among the 3559 predictive curves of one sample in Figure S.8 in Section S.3.3 of supplementary material.

Using the fMRI time series curves of the 3559 voxels as functional predictors, we apply the methods in Simulation 4 to fit the model. Based on 100 iterations as in the study using ROI curves, the average (standard deviation) of the MSPEs are 0.176(0.029) for our method *new.SmSp*, 1.023(0.175) for *wLasso* and 1.044(0.186) for *wwLasso*. Compared to the model using 68 ROIs, when using $p = 3559$ voxels, the prediction error of our method decreases greatly. This implies that information is lost when taking average of the voxel time series in each ROI. Among the 3559 voxels, 49 of them are selected more than 90% times, and 97 are selected more than 80% times. These selected voxels are sparse and does not show a structured clustering. A possible way to improve the voxel selection is to incorporate a group penalty in the simultaneous sparse-smooth penalty (3.7), where the group refers to the ROI information. This will be explored in future study.

References

Aguilera, A. M., Escabias, M., Preda, C. and Saporta, G. (2010) Using basis expansions for estimating functional pls regression: applications with chemometric data. *Chemometrics and Intelligent Laboratory Systems*, **104**, 289–305.

Ait-Saïdi, A., Ferraty, F., Kassa, R. and Vieu, P. (2008) Cross-validated estimations in the single-functional index model. *Statistics*, **42**, 475–494.

Ashburner, J., Barnes, G., Chen, C., Daunizeau, J., Flandin, G., Friston, K., Kiebel, S., Kilner, J., Litvak, V., Moran, R. *et al.* (2014) Spm12 manual. *Wellcome Trust Centre for Neuroimaging, London (UK)*.

Benko, M., Härdle, W., Kneip, A. *et al.* (2009) Common functional principal components. *The Annals of Statistics*, **37**, 1–34.

Boulesteix, A.-L. and Strimmer, K. (2006) Partial least squares: a versatile tool for the analysis of high-dimensional genomic data. *Briefings in Bioinformatics*, **8**, 32–44.

Brodmann, K. (1909) *Vergleichende Lokalisationslehre der Grosshirnrinde in ihren Prinzipien dargestellt auf Grund des Zellenbaues*. Barth.

Brosch, M., Budinger, E. and Scheich, H. (2002) Stimulus-related gamma oscillations in primate auditory cortex. *Journal of Neurophysiology*, **87**, 2715–2725.

Brown, P. J., Fearn, T. and Vannucci, M. (2001) Bayesian wavelet regression on curves with application to a spectroscopic calibration problem. *Journal of the American Statistical Association*, **96**, 398–408.

Cardot, H., Ferraty, F., Mas, A. and Sarda, P. (2003a) Testing hypotheses in the functional linear model. *Scandinavian Journal of Statistics*, **30**, 241–255.

Cardot, H., Ferraty, F. and Sarda, P. (1999) Functional linear model. *Statistics and Probability Letters*, **45**, 11–22.

Cardot, H., Ferraty, F. and Sarda, P. (2003b) Spline estimators for the functional linear model. *Statistica Sinica*, **13**, 571–592.

Chaouch, M., Laïb, N. *et al.* (2013) Nonparametric multivariate $l_{\{1\}}$ -median regression estimation with functional covariates. *Electronic Journal of Statistics*, **7**, 1553–1586.

Chen, D., Hall, P., Müller, H.-G. *et al.* (2011) Single and multiple index functional regression models with nonparametric link. *The Annals of Statistics*, **39**, 1720–1747.

Collazos, J. A., Dias, R. and Zambom, A. Z. (2016) Consistent variable selection for functional regression models. *Journal of Multivariate Analysis*, **146**, 63–71.

Crainiceanu, C. M. and Goldsmith, A. J. (2010) Bayesian functional data analysis using winbugs. *Journal of Statistical Software*, **32**.

Crainiceanu, C. M., Staicu, A.-M. and Di, C.-Z. (2009) Generalized multilevel functional regression. *Journal of the American Statistical Association*, **104**, 1550–1561.

Crambes, C., Kneip, A., Sarda, P. *et al.* (2009) Smoothing splines estimators for functional linear regression. *The Annals of Statistics*, **37**, 35–72.

Delaigle, A., Hall, P. *et al.* (2012) Methodology and theory for partial least squares applied to functional data. *The Annals of Statistics*, **40**, 322–352.

Di, C.-Z., Crainiceanu, C. M., Caffo, B. S. and Punjabi, N. M. (2009) Multilevel functional principal component analysis. *The Annals of Applied Statistics*, **3**, 458.

Edwards, E., Soltani, M., Deouell, L. Y., Berger, M. S. and Knight, R. T. (2005) High gamma activity in response to deviant auditory stimuli recorded directly from human cortex. *Journal of Neurophysiology*, **94**, 4269–4280.

Eilers, P. H., Li, B. and Marx, B. D. (2009) Multivariate calibration with single-index signal regression. *Chemometrics and Intelligent Laboratory Systems*, **96**, 196–202.

Engel, A. K., König, P., Kreiter, A. K. and Singer, W. (1991) Interhemispheric synchronization of oscillatory neuronal responses in cat visual cortex. *Science*, **252**, 1177–1179.

Escabias, M., Aguilera, A. M. and Valderrama, M. J. (2007) Functional pls logit regression model. *Computational Statistics & Data Analysis*, **51**, 4891–4902.

Febrero-Bande, M., de la Fuente, M. O. *et al.* (2012) Statistical computing in functional data analysis: The r package fda. usc. *Journal of Statistical Software*, **51**, 1–28.

Fengler, M. R., Härdle, W. K. and Villa, C. (2003) The dynamics of implied volatilities: A common principal components approach. *Review of Derivatives Research*, **6**, 179–202.

Ferraty, F., Goia, A., Salinelli, E. and Vieu, P. (2013) Functional projection pursuit regression. *Test*, **22**, 293–320.

Ferraty, F., Park, J. and Vieu, P. (2011) Estimation of a functional single index model. In *Recent Advances in Functional Data Analysis and Related Topics*, 111–116. Springer.

Ferraty, F. and Vieu, P. (2002) The functional nonparametric model and application to spectrometric data. *Computational Statistics*, **17**, 545–564.

Ferraty, F. and Vieu, P. (2006a) *Nonparametric Functional Data Analysis: Theory and Practice*. Springer.

Ferraty, F. and Vieu, P. (2006b) *Nonparametric functional data analysis: theory and practice*. Springer Science & Business Media.

Ferré, L. and Yao, A.-F. (2003) Functional sliced inverse regression analysis. *Statistics*, **37**, 475–488.

Ferré, L. and Yao, A.-F. (2005) Smoothed functional inverse regression. *Statistica Sinica*, 665–683.

Fries, P., Reynolds, J. H., Rorie, A. E. and Desimone, R. (2001) Modulation of oscillatory neuronal synchronization by selective visual attention. *Science*, **291**, 1560–1563.

Goldsmith, J., Bobb, J., Crainiceanu, C. M., Caffo, B. and Reich, D. (2011) Penalized functional regression. *Journal of Computational and Graphical Statistics*, **20**.

Goutis, C. and Fearn, T. (1996) Partial least squares regression on smooth factors. *Journal of the American Statistical Association*, **91**, 627–632.

Gray, C. M., König, P., Engel, A. K., Singer, W. *et al.* (1989) Oscillatory responses in cat visual cortex exhibit inter-columnar synchronization which reflects global stimulus properties. *Nature*, **338**, 334–337.

Greven, S., Crainiceanu, C., Caffo, B. and Reich, D. (2011) Longitudinal functional principal component analysis. In *Recent Advances in Functional Data Analysis and Related Topics*, 149–154. Springer.

Hall, P., Horowitz, J. L. *et al.* (2007) Methodology and convergence rates for functional linear regression. *The Annals of Statistics*, **35**, 70–91.

Hall, P. and Vial, C. (2006) Assessing the finite dimensionality of functional data. *Journal of the Royal Statistical Society: Series B (Statistical Methodology)*, **68**, 689–705.

Hilgert, N., Mas, A., Verzelen, N. *et al.* (2013) Minimax adaptive tests for the functional linear model. *The Annals of Statistics*, **41**, 838–869.

Horváth, L. and Kokoszka, P. (2012) *Inference for Functional Data with Applications*, vol. 200. Springer Science & Business Media.

Hosseini-Nasab, M. (2013) Cross-validation approximation in functional linear regression. *Journal of Statistical Computation and Simulation*, **83**, 1429–1439.

James, G. M. and Silverman, B. W. (2005) Functional adaptive model estimation. *Journal of the American Statistical Association*, **100**, 565–576.

Kneip, A. and Utikal, K. J. (2001) Inference for density families using functional principal component analysis. *Journal of the American Statistical Association*, **96**, 519–542.

Kong, D., Staicu, A.-M. and Maity, A. (2016a) Classical testing in functional linear models. *Journal of Nonparametric Statistics*, **28**, 813–838.

Kong, D., Xue, K., Yao, F. and Zhang, H. H. (2016b) Partially functional linear regression in high dimensions. *Biometrika*, **103**, 147–159.

Krämer, N., Boulesteix, A.-L. and Tutz, G. (2008) Penalized partial least squares with applications to b-spline transformations and functional data. *Chemometrics and Intelligent Laboratory Systems*, **94**, 60–69.

Krämer, N. and Sugiyama, M. (2011) The degrees of freedom of partial least squares regression. *Journal of the American Statistical Association*, **106**, 697–705.

Lancaster, J., Summerln, J., Rainey, L., Freitas, C. and Fox, P. (1997) The talairach daemon, a database server for talairach atlas labels. *Neuroimage*, **5**, S633.

Lancaster, J. L., Woldorff, M. G., Parsons, L. M., Liotti, M., Freitas, C. S., Rainey, L., Kochunov, P. V., Nickerson, D., Mikiten, S. A. and Fox, P. T. (2000) Automated talairach atlas labels for functional brain mapping. *Human brain mapping*, **10**, 120–131.

Li, Y., Wang, N. and Carroll, R. J. (2013) Selecting the number of principal components in functional data. *Journal of the American Statistical Association*, **108**, 1284–1294.

Lian, H. (2013) Shrinkage estimation and selection for multiple functional regression. *Statistica Sinica*, 51–74.

Maldjian, J. A., Laurienti, P. J., Kraft, R. A. and Burdette, J. H. (2003) An automated method for neuroanatomic and cytoarchitectonic atlas-based interrogation of fmri data sets. *Neuroimage*, **19**, 1233–1239.

Marx, B. D. and Eilers, P. H. (1999) Generalized linear regression on sampled signals and curves: a p-spline approach. *Technometrics*, **41**, 1–13.

Matsui, H., Araki, Y. and Konishi, S. (2008) Multivariate regression modeling for functional data. *Journal of Data Science*, **6**, 313–331.

Mitra Lab in Cold Spring Harbor Laboratory (2014) Chronux analysis software. <http://chronux.org/>.

Morris, J. S. (2015) Functional regression. *Annual Review of Statistics and Its Application*, **2**, 321–359.

O'Hagan, A. and Kingman, J. F. C. (1978) Curve fitting and optimal design for prediction. *Journal of the Royal Statistical Society. Series B (Methodological)*, 1–42.

Preda, C. and Saporta, G. (2005) Pls regression on a stochastic process. *Computational Statistics & Data Analysis*, **48**, 149–158.

Rachdi, M. and Vieu, P. (2007) Nonparametric regression for functional data: automatic smoothing parameter selection. *Journal of Statistical Planning and Inference*, **137**, 2784–2801.

Ramsay, J. O. and Dalzell, C. (1991) Some tools for functional data analysis. *Journal of the Royal Statistical Society. Series B (Methodological)*, 539–572.

Ramsay, J. O. and Silverman, B. W. (2005) *Functional Data Analysis. 2nd Edition.* New York: Springer.

Rasmussen, C. E. and Williams, C. K. (2006) Gaussian processes for machine learning. 2006. *The MIT Press, Cambridge, MA, USA*, **38**, 715–719.

Reiss, P. T., Goldsmith, J., Shang, H. L. and Ogden, R. T. (2017) Methods for scalar-on-function regression. *International Statistical Review*, **85**, 228–249.

Reiss, P. T., Huo, L., Zhao, Y., Kelly, C. and Ogden, R. T. (2015) Wavelet-domain regression and predictive inference in psychiatric neuroimaging. *The Annals of Applied Statistics*, **9**, 1076.

Reiss, P. T. and Ogden, R. T. (2007) Functional principal component regression and functional partial least squares. *Journal of the American Statistical Association*, **102**, 984–996.

Rice, J. A. and Silverman, B. W. (1991) Estimating the mean and covariance structure nonparametrically whe the data are curves. *J. Roy. Statist. Soc. Ser. B*, **53**, 233–243.

Ruppert, D., Wand, M. P. and Carroll, R. J. (2003) Semiparametric regression. cambridge series in statistical and probabilistic mathematics 12. *Cambridge: Cambridge Univ. Press.* *Mathematical Reviews (MathSciNet): MR1998720.*

Shang, H. L. (2013) Bayesian bandwidth estimation for a nonparametric functional regression model with unknown error density. *Computational Statistics & Data Analysis*, **67**, 185–198.

Silverman, B. W. (1996) Smoothed functional principal components analysis by choice of norm. *The Annals of Statistics*, **24**, 1–24.

Su, Y.-R., Di, C.-Z. and Hsu, L. (2017) Hypothesis testing in functional linear models. *Biometrics*, **73**, 551–561.

Swihart, B. J., Goldsmith, J. and Crainiceanu, C. M. (2014) Restricted likelihood ratio tests for functional effects in the functional linear model. *Technometrics*, **56**, 483–493.

ter Braak, C. J. and de Jong, S. (1998) The objective function of partial least squares regression. *Journal of Chemometrics*, **12**, 41–54.

Wahba, G. (1990) *Spline Models for Observational Data*. Society for Industrial and Applied Mathematics.

Walz, J. M., Goldman, R. I., Carapezza, M., Muraskin, J., Brown, T. R. and Sajda, P. (2013) Simultaneous eeg-fmri reveals temporal evolution of coupling between supramodal cortical attention networks and the brainstem. *Journal of Neuroscience*, **33**, 19212–19222.

Wang, B., Chen, T. and Xu, A. (2017) Gaussian process regression with functional covariates and multivariate response. *Chemometrics and Intelligent Laboratory Systems*, **163**, 1–6.

Wang, J.-L., Chiou, J.-M. and Müller, H.-G. (2016) Functional data analysis. *Annual Review of Statistics and Its Application*, **3**, 257–295.

Wold, H. (1973) Nonlinear iterative partial least squares (nipals) modelling: some current developments. In *Multivariate Analysis-III*, 383–407. Elsevier.

Wold, H. (1975) Path models with latent variables: The nipals approach. In *Quantitative Sociology*, 307–357. Elsevier.

Womelsdorf, T., Fries, P., Mitra, P. P. and Desimone, R. (2006) Gamma-band synchronization in visual cortex predicts speed of change detection. *Nature*, **439**, 733–736.

Wood, S. N. (2011) Fast stable restricted maximum likelihood and marginal likelihood estimation of semiparametric generalized linear models. *Journal of the Royal Statistical Society: Series B (Statistical Methodology)*, **73**, 3–36.

Yao, F., Müller, H. G. and Wang, J. L. (2005a) Functional data analysis for sparse longitudinal data. *Journal of the American Statistical Association*, **100**, 577–590.

Yao, F., Müller, H.-G. and Wang, J.-L. (2005b) Functional linear regression analysis for longitudinal data. *The Annals of Statistics*, **33**, 2873–2903.

Zhang, X., King, M. L. and Shang, H. L. (2014) A sampling algorithm for bandwidth estimation in a nonparametric regression model with a flexible error density. *Computational Statistics & Data Analysis*, **78**, 218–234.

Zhao, Y., Chen, H. and Ogden, R. T. (2015) Wavelet-based weighted lasso and screening approaches in functional linear regression. *Journal of Computational and Graphical Statistics*, **24**, 655–675.

Zhao, Y., Ogden, R. T. and Reiss, P. T. (2012) Wavelet-based lasso in functional linear regression. *Journal of Computational and Graphical Statistics*, **21**, 600–617.

Zhu, H. and Cox, D. D. (2009) A functional generalized linear model with curve selection in cervical pre-cancer diagnosis using fluorescence spectroscopy. *Lecture Notes-Monograph Series*, 173–189.

Zou, H. and Hastie, T. (2005) Regularization and variable selection via the elastic net. *Journal of Royal Statistical Society: Series B (Statistical Methodology)*, **67**, 301–320.